

₁ Proposal for a Full-Scale Detector Engineering Test
₂ and Test Beam Calibration of a Single-Phase LAr
₃ TPC

₄ A. name1¹, B. name2², and C. name3³

₅ ¹Department of X1, University Y1

₆ ²Department of X2, University Y2

₇ ³Department of X3, University YY3

₈ February 24, 2015

₉ **Abstract**

₁₀ insert abstract here

11 Contents

12	1 Introduction [~5 pages; Thomas/Greg/Bob Wilson]	4
13	1.1 Physics goals of LBNF	4
14	1.2 Single-phase LAr TPC Prototype	4
15	1.3 Goals for the prototype run	5
16	2 CERN prototype detector and charged particle beam test [~10 pages; Donna/Jarek]	5
18	2.1 Requirements for the detector, beam and commissioning	5
19	2.2 Detector performance tests	9
20	2.3 Other measurements	11
21	3 Single Phase LAr Detector [~10 pages; J. Stewart et al.]	11
22	3.1 LBNF detector	11
23	3.2 CERN prototype detector	13
24	3.3 Introduction	23
25	3.4 Baseline Design (TPB-Coated Acrylic Bars)	24
26	3.5 Alternate 1: Coated Acrylic Plate with Fiber Readout	24
27	3.6 Alternate 2: Fiber Bundle with TPB-coated radiator	24
28	3.7 Technology Selection	25
29	4 Cryostat and cryogenics system [~5 pages; David/Barry/Jack]	26
30	4.1 LBNF detector	26
31	4.2 CERN prototype detector	26
32	4.3 Cryogenic System (from David Montanari)	33
33	5 Charged Particle Test Beam Requirements [~10 pages; Cheng-Ju]	35
34	5.1 Particle Beam Requirements	35
35	5.2 EHN1 H4ext Beamline	35
36	5.3 Beam Instrumentation	36
37	5.4 Muon Beam Halo Counters	36
38	5.5 Beam Window on LAr Cryostat	36
39	6 Computing requirements, data handling and software [~3 pages; Maxim Potekhin/Craig Tull]	36
41	6.1 Overview	36
42	6.2 Collecting and Storing Raw Data	37
43	6.3 Databases	40
44	6.4 A note on Simulation and Reconstruction Software	40
45	6.5 Distributed Computing, Workload and Workflow Management	41
46	7 CERN neutrino platform test environment [5 pages; David/Jack/Cheng-Ju/Thomas]	43
48	8 Organization, schedule and cost estimate [~5 pages; Thomas/Greg]	43

49 9 Summary [\sim 2 pages; Thomas/Greg]

43

50 **1 Introduction** [~5 pages; Thomas/Greg/Bob Wil-
51 son]

52 This document is a technical report for the Expression of Interest <reference> submitted
53 to the CERN SPSC in October 2014. In this report, we detail the proposal to test full-
54 scale detector elements for a single-phase liquid argon (LAr) TPC based on the former
55 LBNE design which is a potential viable technology for use as a far detector for the
56 experiment that will be at the Long Baseline Neutrino Facility (LBNF). To mitigate
57 the risks associated with extrapolating small scale versions of the single-phase LAr TPC
58 technology to a full-scale detector element, it is essential to benchmark the operation of a
59 full-scale detector elements in a particle beam. The beam facility at the CERN Neutrino
60 Platform (cite) provides an opportunity to perform this crucial test of the proposed
61 single-phase LAr TPC and inform the decision regarding phased implementation of the
62 far detector for LBNF.

63 **1.1 Physics goals of LBNF**

64 An international collaboration is forming that will utilize a proposed 1.2 MW proton
65 beam at FNAL to create a neutrino beam that will be directed at the Homestake Mine
66 in the USA. The proposal is to place by the year 2024 <mention 2021 date for 10kton>
67 a 40 kton LAr TPC in the underground facility at Homestake to observe the oscillation
68 of $\nu_\mu \rightarrow \nu_e$ and $\bar{\nu}_\mu \rightarrow \bar{\nu}_e$ that occur near a neutrino energy of 3 GeV and thereby make
69 precision measurements of δ_{CP} , δ_{13} , and δ_{23} and determining the neutrino mass hierarchy.
70 In order to make such precise measurements, the detector will need to accurately identify
71 and measure the energy of the particles produced in the neutrino interaction with Argon
72 which will range from a few GeV to hundreds of MeV.

73 **1.2 Single-phase LAr TPC Prototype**

74 The LBNE-style single-phase LAr TPC is design to be scalable using module units that
75 consist of a factory-built anode plane, a cathode a plane, and a field cage with the anode
76 plane assemblies measuring 6.0m (h) \times 2.3m (w) \times 0.09m (d) and a drift length of 2.5m.
77 The electronics will be mounted in the cryostat on the wire planes to reduce the number
78 of cables that penetrate the cryostat and optimize the electronic signal to noise. Event
79 timing will be determined through the use of scintillation photon detectors that will use
80 light collection paddles. With this modular design as shown in <insert figure of LBNE
81 detector to shown modular design> , it will be possible to achieve the goal of 40 kton
82 detector for the LBNF far site.

83 Some features of this single-phase design will be tested using smaller scale prototypes
84 such as the ongoing tests with a 35ton unit at Fermilab and the 5ton CAPTAIN LAr
85 TPC. However, none of these smaller prototypes uses full scale detector elements or
86 are large enough to fully contain particles. Considering that the detector at the LBNF
87 far site will be about a factor of 50 larger in scale than the ICARUS detector which
88 is currently the largest LAr TPC detector built to date, it is essential to validate the
89 full-scale detector elements in a particle beam at the CERN Neutrino Platform.

90 In order to fully contain particles within the energy range of interest and provide
91 space for detector services, the cryostat will need to have a minimum inner dimensions
92 of 8.4m (h) \times 7.3m (w) \times 9.5m (d). It is anticipated that the CERN Neutrino Platform
93 will facilitate the design and construction of the cryostat and that this effort will common
94 area that will motivate collaboration with the WA105 team.

95 1.3 Goals for the prototype run

96 The goals of the prototype run include:

- 97 • Use of particle beam to assess
 - 98 tracking and calorimetric response
 - 99 reconstruction algorithm
 - 100 Monte Carlo simulation
 - 101 Secondary hadron interactions in detector
- 102 • Verifying argon contamination mitigation
- 103 • Full-scale structural test under LAr cryogenic conditions
- 104 • Verification of TPC Electrics under LAr cryogenic conditions
- 105 • Study light levels of the photon detection system
- 106 • Developing installation procedures for full-scale electronics

107 2 CERN prototype detector and charged particle 108 beam test [\sim 10 pages; **Donna/Jarek**]

109 describe and motivate proposed detector and beam test requirements

110 2.1 Requirements for the detector, beam and commissioning

111 The Single-Phase Cern Prototype detector is intended to provide necessary information
112 to reduce systematic uncertainties for the oscillation measurements in the US-based
113 long base-line neutrino experiment. The LAr TPC technology is not new but wasn't
114 extensively used in the 1-10 GeV neutrino energy range. The main source of uncertainties
115 due to detector with the current values are shown in table 1

116 With current detector uncertainties from table 1 the sensitivities for the CP violation
117 phase measurement is shown in Fig. 2.1 **Task: make this plot**. The proposed test
118 beam detector will reduce uncertainties to XX% and improve our sensitivity to δ_{CP} as
119 shown in Fig. 2.1 **Task: make this plot**.

Table 1: Current known sources of detector uncertainties for liquid argon or TPC.

source of uncertainty	value	reference
e/ γ separation		
e-m shower calibration		
hadronic shower calibration		
low energy acceptance electron identification		
.....		

Table 2: Current known sources of uncertainties due to interaction of charged particle with argon.

source of uncertainty	value	reference
pion(Kaon) absorbtion		
pion(Kaon) charge exchange		
pion (Kaon) production in secondary interactions		
muon capture		Phys. Rev. C 35, 2212
energy scale		
Michel electron tagging		
.....		

Figure 1: Sensitivities for the δ_{CP} measurement for using current knowledge of the single-phase LAr-TPC detector technology and for reduced detector uncertainties from SPCP beamtest data. The plots prepared for 40 kton fiducial mass and $xx \times 10^{21}$ POT.

¹²⁰ 2.1.1 Particles energy and direction

¹²¹ Plans for running beam for the the ELBNF include both neutrino and anti-neutrino
¹²² configurations. These beams will be composed mainly of muon neutrinos (anti-neutrinos)
¹²³ as well as electron neutrinos (anti-neutrinos). In figures 2.1.1 and 2.1.1 the distributions
¹²⁴ on momenta and angles of particles created in neutrino interaction are shown.

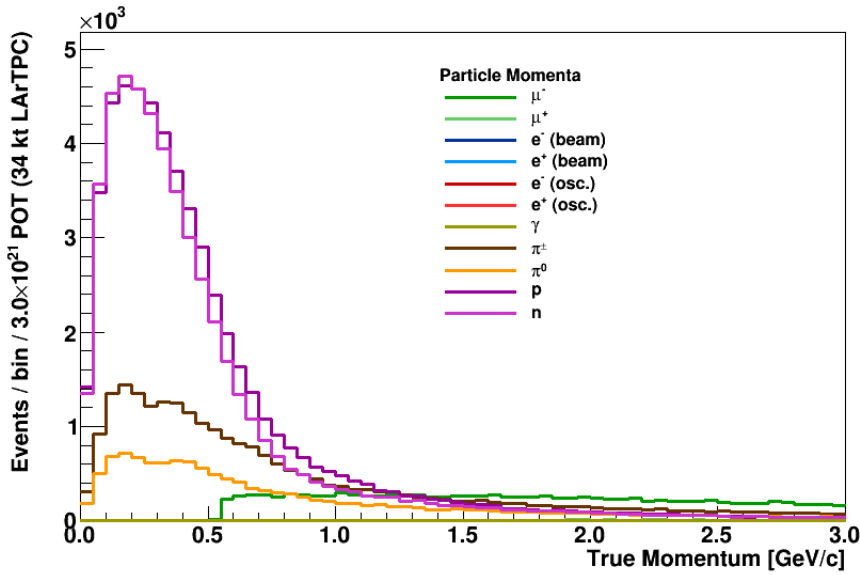


Figure 2: Particle momenta distributions for particles coming from all fluxes (ν_e , ν_μ , $\bar{\nu}_e$ and $\bar{\nu}_\mu$) at both near and far detector locations.

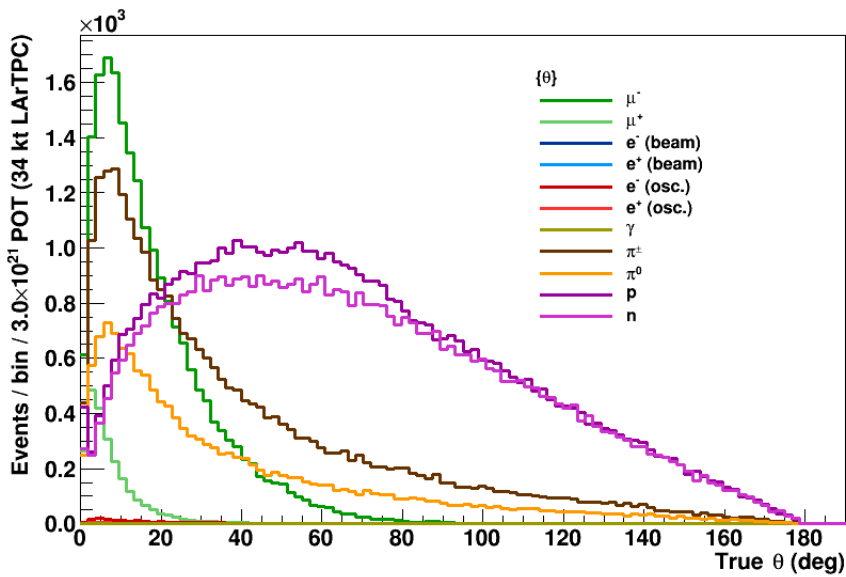


Figure 3: Particle angle wrt to the beam axis distributions for particles coming from all fluxes (ν_e , ν_μ , $\bar{\nu}_e$ and $\bar{\nu}_\mu$) at both near and far detector locations.

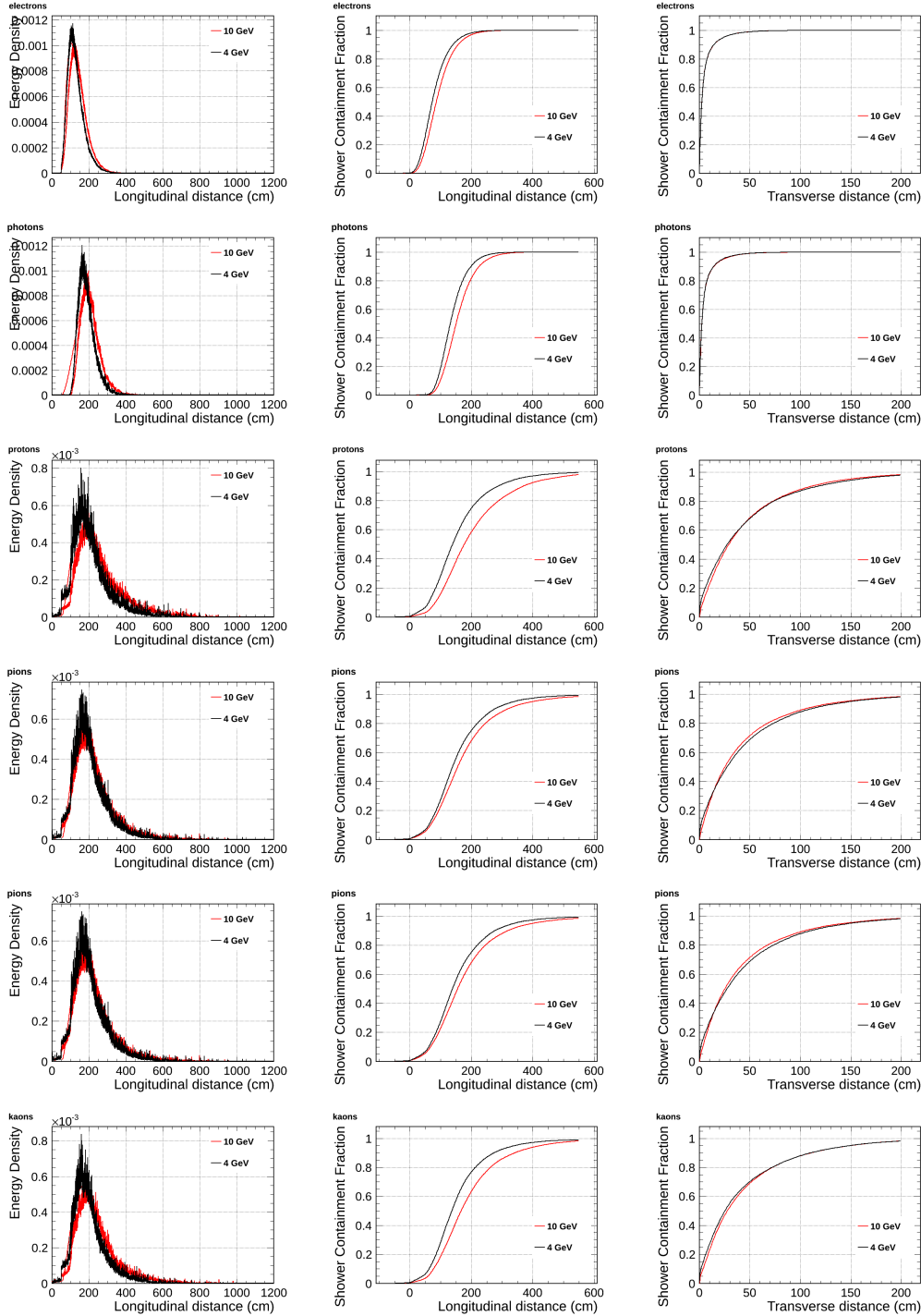


Figure 4: Particle containment plots.

125 **2.1.2 Particle rates**

126 Estimation of beam particles rates necessary to collect high enough statistics in a rea-
127 sonable time to obtain goals of the measurements.

128 **2.1.3 Run plan**

129 Based of the rates from the beam and required rates from the physics considerations.

130 **2.2 Detector performance tests**

131 **2.2.1 Bethe-Bloch parametrisation of charged particles**

132 The SPCP will allow to study the detector response to charge particles from the test
133 beam and will serve as a calibration detector. The measured energy deposition for
134 various particles and its dependence on the direction of the particle will feed into our
135 Monte Carlo generator and allow more precise reconstruction of neutrino energy and
136 interactions topologies with good particle identifications.

137 **How we compare with Lariat? Multiple scattering**

138 The set of single-phase prototype detector helped to understand the detector response
139 to cosmic muons. But there is still lots to learn with additional studies. The charge
140 particle identification efficiencies has been mapped for only limited range of the particle
141 energies.

142 **2.2.2 e/ γ separation**

143 The separation of the electrons from photons is the most important feature of the LAr
144 TPC detectors for the search of the CP violation phase where we look for appearance of
145 the ν_e in the ν_μ beam. Showers from electrons are part of the signal whilst the single pho-
146 tons might contribute to the background sample. The photons can undergo two process:
147 pair production and Compton scattering. The dominant process for photons with ener-
148 gies of several hundreds MeV is the $e^+ e^-$ pair production, but Compton scattering also
149 occur at this energies. For pair production the e/γ separation is achieved by looking at
150 the beginning of the electromagnetic shower, where for election we see energy deposition
151 typical for single MIP and for photon we see energy deposition consisted with two MIP.
152 The separation of e/γ has been measured in the ArgoNEUT experiment using neutrino
153 scattering data with low statistics. Currently the separation efficiency is estimated to be
154 at the level of of 94 % (? cite and check the number). In case of the Compton scattering
155 the off atomic electron the signal is much more difficult to distinguish from the electron
156 from the CC ν_e scattering.

157 The separation of the e/γ measured by ArgoNEUT is not sufficient for the ELBNF
158 experiment. Here we propose a measurement of the separation efficiency as the function
159 of energy and angle. **we need someone to look into this**

160 **2.2.3 Reconstruction efficiencies and particle identification**

161 The reconstruction of events in the LAr TPC is still a challenge but rapid progress has
162 been achieved in recent years (cite pandora and other reconstruction algorithms). De-

¹⁶³ spite the progress reconstruction algorithms have to rely Monte Carlo predictions which
¹⁶⁴ don't simulate liquid argon detectors responses correctly. Reconstruction algorithms
¹⁶⁵ will benefit greatly from test beam data particularly from the full scale prototype. The
¹⁶⁶ reconstruction algorithms will be trained to correctly reconstruct track, electromagnetic
¹⁶⁷ and hadronic showers.

¹⁶⁸ The data of tracks and showers can be used to create a library which can be used
¹⁶⁹ for matching with he neutrino data, similar to the LEM (library event matching).

¹⁷⁰ Main issues for the reconstruction algorithms:

- ¹⁷¹ • The reconstruction algorithms try to use all three planes on the signal readout. if
¹⁷² the orientation of the track/shower is such that it is aligned with wires on one of
¹⁷³ the plans it significantly reduces quality of reconstructed objects.
- ¹⁷⁴ • Calorimetry with collection and induction planes. In the ICARUS experiment the
¹⁷⁵ deposited energy was reconstructed from the signal on the collection plane. The
¹⁷⁶ induction planes bipolar signal wasn't "stable" enough to use it for calorimetric
¹⁷⁷ measurement. In the ELBNF design there is additional shielding wire plane which
¹⁷⁸ will improve the quality of the bipolar signal and the test beam experiment will
¹⁷⁹ help with its calibration.
- ¹⁸⁰ • Vertexing.
- ¹⁸¹ • Reconstruction efficiency for low energy particles. The reconstruction algorithm
¹⁸² suffer from the lose of fefficiency for low energy particle or particles which leave
¹⁸³ less than 200-300 hits. Training the algorithms on a low energy particles from the
¹⁸⁴ test beam will improve the quality and efficiency of the reconstructed objects.

¹⁸⁵ 2.2.4 Cross section measurements

¹⁸⁶ Precise measurement of the absorption and charge exchange of pions and kaons. Pion
¹⁸⁷ absorption is a large part of the pion nucleon cross section from 50 MeV to 500MeV with
¹⁸⁸ no data above about 1GeV pion kinetic energy. **Add plots and values for known**
¹⁸⁹ **cross sections wit errors**

- ¹⁹⁰ • pion absorption on argon - Kotlinski, EPJ 9, 537 (2000)
- ¹⁹¹ • pion cross section as a function of A - Gianelli PRC 61, 054615 (2000)

¹⁹² There is not currently a satisfactory theory describing absorption. The Valencia group
¹⁹³ (Vicente-Vacus NPA 568, 855 (1994)) developed model of the pion-nucleus reaction with
¹⁹⁴ fairly good agreement, although not in detail. The actual mechanism of multi-nucleon
¹⁹⁵ absorption is not well understood.

¹⁹⁶ 2.2.5 Charge sign determination

¹⁹⁷ It is not possible to determine charge of the particle on the event by event basis with non-
¹⁹⁸ magnetised LAr TPC detectors. However, the statistical analyst will be possible. We
¹⁹⁹ will fit the muon's half time which is different for muons and antimony due to different
²⁰⁰ muon capture cross sections. For the μ^+ for argon we expect about xx% to be captured
²⁰¹ and for μ^- about yy%.

202 **2.2.6 Single track calibration**

203 **2.2.7 Shower calibration**

204 Reconstruction of neutrino energy depends of a quality of reconstruction of both elec-
205 tromagnetic and hadronic showers.

206 - **features of Hadronic shower in LAr TPC - features of electromagnetic**
207 **shower in LAr TPC - Missing energy from neutral (Neutrons scattering)**

208 **2.3 Other measurements**

209 **2.3.1 Anti-proton annihilation**

210 **2.3.2 Proton decay background (cosmogenic $K^0 \rightarrow K^+$)**

211 **3 Single Phase LAr Detector [\sim 10 pages; J. Stewart
et al.]**

213 **3.1 LBNF detector**

214 The far detector for the ELBNF collaboration will be a series of four xx kt (10 kt) ac-
215 tive (fiducial) volume liquid argon time projection chambers instrumented with photon
216 detection. It is planned that the first 10 kt detector will be ready for commissioning in
217 2021. One option for the TPC design is a wire plane based TPC with cold electron-
218 ics readout. Designs of this style are referred to as single-phase detectors as the
219 charge generation, drift, and detection all occurs in the argon liquid phase. This style
220 TPC has the advantage that there is no charge amplification before collection making a
221 very precise charge measurement possible. To achieve ELBNF's goals, a detector much
222 larger than ICARUS, the largest LAr TPC detector built to date, is needed. ELBNE
223 is developing a scalable far detector design shown in Figure 5 that would scale-up LAr
224 TPC technology by roughly a factor of 50 compared to the ICARUS T600 detector.
225 To achieve this scale-up, a number of novel design elements need to be employed. A
226 membrane cryostat typical for the liquefied natural gas industry will be used instead of
227 a conventional evacuated cryostat. The wire planes or anode plane assemblies (APAs)
228 will be factory-built as planar modules that are then installed into the cryostat. The
229 modular nature of the APAs allow the size of the detector to be scaled up to at least
230 40 kt fiducial mass. Both the analog and digital electronics will be mounted on the wire
231 planes inside the cryostat in order to reduce the electronic noise, to avoid transporting
232 analog signals large distances, and to reduce the number of cables that penetrate the
233 cryostat. The scintillation photon detectors will employ light collection paddles to re-
234 duce the required photo-cathode area. Many of the aspects of the design will be tested
235 in a small scale prototype at Fermilab but given the very large scale of the detector
236 elements a full-scale test is highly desirable.

237 The goals of the LBNE detector test can be broken into four categories: argon
238 contamination mitigation verification, TPC mechanical verification, TPC electrical veri-
239 fication, and photon detection light yield verification. Research at Fermilab utilizing the
240 Materials Test Stand has shown that electronegative contamination to the ultra-pure

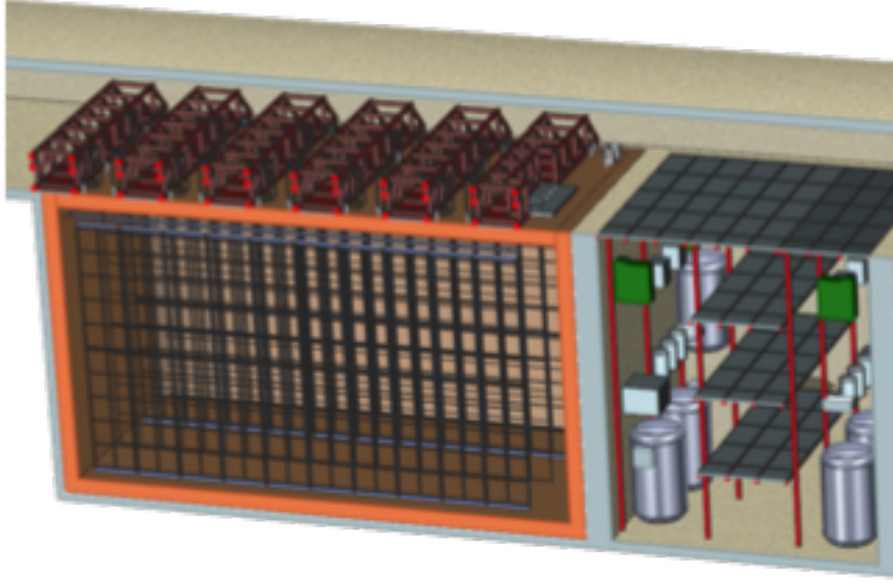


Figure 5: 3D model of one design of the ELBNF single-phase detector. Shown is 5kt fiducial volume detector which would need to be lengthened for the 10 kt design. The present ELBNF plan calls for the construction of 4 10 kt detectors of similar design.

241 argon from all materials tested is negligible if the material is under the liquid argon.
 242 This implies that the dominant source of contamination originates from the gas ullage
 243 region and in the room temperature connections to the detector. Careful design of the
 244 ullage region to insure that all surfaces and feedthroughs are cold is expected to greatly
 245 reduce the sources of contamination over what exists in present detectors. Other con-
 246 cepts attempt to eliminate the gas ullage completely. The goals related to mechanical
 247 testing are to test the integrity of the detector. In the current design, each APA mea-
 248 sures 2.3 m by 6.0 m and includes 2560 wires and associated readout channels. Given
 249 the complexity of these assemblies, a test where the detector can be thermally cycled
 250 and tested under operating conditions is highly advised prior to mass production. The
 251 mechanical support of the APAs can be tested to verify that the mechanical design is
 252 reliable and will accommodate any necessary motion between the large wire planes. The
 253 impact of vibration isolation between the cryostat roof and the detector can also be
 254 tested. Finally a potential improvement in the cryostat design is the possibility to move
 255 the pumps external to the main cryostat. This will reduce any mechanical coupling to
 256 the detector and also greatly improve both reliability and ease of repair. The electrical
 257 testing goals are to insure that the high voltage design is robust and that the required
 258 low electronic noise level can be achieved. As the detector scale increases so does the
 259 capacitance and the stored energy in the device. The design of the field cage and high
 260 voltage cathode planes needs to be such that HV discharge is unlikely and that if the
 261 event occurs no damage to the detector or cryostat results. The grounding and shield-
 262 ing of large detectors is also critical for low noise operation. By testing the full scale
 263 elements one insures that the grounding plan is fully developed and functional. Large
 264 scale tests of the resulting design will verify the electrical model of the detector.

265 **3.2 CERN prototype detector**

266 **3.2.1 Overview of the CERN test Detector**

267 The TPC will be assembled from elements that are of the same size as those planned
268 for the single phase far detector. The overall size of the TPC will be derived by the
269 size and number of anode planes (APA). It has been determined in order to perform the
270 required physics, the TPC will consist of three APAs. The APAs will have an active
271 area 2.29 m wide and 6.0 m high. These active area dimensions result in an APA that
272 is 2.32 m wide and 6.29 m high. The combination of the three APAs will determine
273 the overall length of the TPC. This is 7.2 m. There will be a cathode plane (CPA) on
274 either side of the APAs. The size of the CPAs is determined by the active area of the
275 three APAs. The active area of the three APAs is approximately 7.2 m wide by 6.2 m
276 high. The drift distance between the CPAs and row of APAs will be 2.5 m. The overall
277 width of the TPC will be determined by a combination of the drift distances along with
278 the thickness of the APA, which is constructed of 3" x 4" stainless steel (SS) structural
279 tubing. The overall width of the TPC is 5.2 m. Like the length of the TPC, the overall
280 height will be determined by the height of the APA. The overall height of the TPC will
281 be 6.3 m. The TPC dimensions will be 7.2 m long x 5.2 m wide x 6.3 m high. Along
282 with the APAs and CPAs, the TPC will include a field cage that surrounds the entire
283 assembly. It will be designed similarly to the field cage in phase 2 of the 35t experiment
284 at FNAL. This is a series of protruded fiberglass I beams for the structural elements.
285 These I-beams will be tiled with large copper sided FR4 panels to create the field cage.
286 Each panel will be connected with a series of resistors. The field cage will be connected
287 to the CPAs through a capacitor assembly.

288 All of this will be supported by rows of I-beams supported from a mechanical struc-
289 ture above the cryostat. The hangers for these I-beams will pass through the insulated
290 top cap. There will be a series of feed thru flanges in the top cap of the cryostat to bring
291 in and take out services for the TPC. There will be a HV feed thru for each of the CPAs
292 and one signal feed thru for each of the APAs

293 **Cryostat size from TPC dimensions (from Jack Fowler)**

294 The minimum internal size of the cryostat is determined from size of the TPC. At the
295 bottom of the cryostat there needs to be a minimum of 0.3 m between the frame of the
296 CPA and closest point on the SS membrane. This is to prevent high voltage discharge
297 between the CPA and the electrically grounded membrane. It is foreseen that there
298 would be some cryogenic piping and instrumentation under the TPC. There is a height
299 allowance of 0.1 m for this. There will be access and egress space around the outside of
300 the TPC and the membrane walls. On three sides, 1.0 m of space is reserved for this.
301 The final side of the TPC will have piping and instrumentation for the cryogenic system.
302 There will be 1.3 m of space reserved for this.

303 The support system for the TPC will be located at the top between the underside
304 of the cryostat roof and the top of the TPC. The plan is to model this space similar to
305 what is planned for the far site TPC. There will be 0.9 m of ullage space. In order to
306 prevent high voltage discharge, the upper most part of the CPA needs to be submerged a
307 minimum of 0.3 m below the liquid Argon surface. The top of the TPC will be separated
308 from the membrane by a minimum of 1.2 m.

309 Adding all of these to the size of the TPC yields the minimum inner dimensions of

310 the cryostat. A minimally sized cryostat would be 9.5 m long, 7.3 m wide and 8.4 m
311 high. This assumes the TPC will be positioned inside the cryostat with the CPAs and
312 end field cages parallel to the walls of the cryostat. Also there is no space allotted for
313 a beam window to enter the cryostat. Clearance would need to be added if it violates
314 any of the current boundaries listed above. These dimensions also preserve the ability
315 to reverse the order of the APAs and CPAs inside the TPC. The current plan is to have
316 the APAs located in the center of the cryostat with a CPA on each side. Reversing this
317 to have the CPA in the center and APAs on each side may be required to achieve some
318 of the proposed physics. The orientation of the TPC components will be finalized after
319 various scenarios have been sufficiently simulated.

320 **3.2.2 Parameters table**

321 **3.2.3 Requirements (data rate, dimensions, gap to wall, ?)**

322 **3.2.4 Installation**

323 **Installation Plans for the TPC into the Cryostat (from Jack Fowler)**

324 The interior of the cryostat will be prepared prior to the installation of the TPC. A
325 series of support rails will be suspended below the top surface of the cryostat membrane.
326 These will be structurally supported by a truss structure above the cryostat. These
327 supports will pass through the top of the cryostat. They need to be designed to minimize
328 the heat gain into the cryogenic volume. For the CPAs, the rails need to be electrically
329 isolated due to high voltage concerns. To preserve the ability to reverse the order of the
330 TPC components, all of the support rails will be designed to the same set of requirements
331 regarding loads and attachment points.

332 There will be a series of feed thru flanges located along each of the support rails.
333 These will be cryogenic flanges where the services for the TPC components can pass
334 through the top of the cryostat. It is foreseen that each CPA will require one feed thru
335 for the high voltage probe to bring in the drift voltage. The drift voltage is 500 V/cm.
336 For a drift distance of 2.5 m, the probe voltage will be 125 kV. There will be one service
337 feed thru for each of the APAs. These feed thrus will include high speed data, bias
338 voltages for the wire planes, control and power for the cold electronics.

339 The main TPC components will be installed through a large hatch in the top of the
340 cryostat. This is similar to the installation method intended for the detector at the far
341 site. This hatch will have an aperture approximately 2.0 m wide and 3.5 m long. Each
342 APA and CPA panel will be carefully tested after transport into the clean area and
343 before installation into one of the cryostats. Immediately after a panel is installed it will
344 be rechecked. The serial installation of the APAs along the rails means that removing
345 and replacing one of the early panels in the row after others are installed would be very
346 costly in effort and time. Therefore, to minimize the risk of damage, as much work
347 around already installed panels as possible will be completed before proceeding with
348 further panels. The installation sequence is planned to proceed as follows:

- 349 1. Install the monorail or crane in the staging area outside the cryostat, near the
350 equipment hatch.

- 351 2. Install the relay racks on the top of the cryostat and load with the DAQ and power
352 supply crates.
- 353 3. Dress cables from the DAQ on the top of the cryostat to remote racks.
- 354 4. Construct the clean-room enclosure outside the cryostat hatch.
- 355 5. Install the raised-panel floor inside the cryostat.
- 356 6. Insert and assemble the stair tower and scaffolding in the cryostat.
- 357 7. Install the staging platform at the hatch entrance into the cryostat.
- 358 8. Install protection on (or remove) existing cryogenics instrumentation in the cryo-
359 stat.
- 360 9. Install the cryostat feedthroughs and dress cables inside the cryostat along the
361 support beams.
- 362 10. Install TPC panels:
- 363 (a) Install both CPA panels. These will be installed from the floor of the cryostat.
364 Access to the top edge will be required by scaffolding.
- 365 (b) Install and connect HV probe for each of the CPAs.
- 366 (c) Perform electrical tests on the connectivity of the probe to the CPAs.
- 367 (d) Install first end wall of vertical field cage at the non-access end of the cryostat.
368 These will be installed from the floor of the cryostat. Scaffolding will be
369 needed to install the supporting structure and then attach the panels to the
370 structure.
- 371 (e) Test the inner connections of the field cage panels.
- 372 (f) Install the first APA and connect to the far end field cage support.
- 373 (g) Connect power and signal cables. This will require scaffolding to access the
374 top edge of the APA.
- 375 (h) Test each APA wire for expected electronics noise. Spot-check electronics
376 noise while cryogenics equipment is operating.
- 377 (i) Install the upper field cage panels for the first APA between the APA and
378 CPAs. This will require scaffolding to access the upper edge of the APA, CPA
379 and field cage structure.
- 380 (j) Perform electrical tests on upper field cage panels.
- 381 (k) Repeat steps (f) through (j) for the next two APAs.
- 382 (l) Install the lower field cage panels between the APAs and CPAs. Start at the
383 far end away from the access hatch and work towards the hatch.
- 384 (m) Perform electrical test on lower field cage panels and the entire loop around
385 the TPC.
- 386 (n) Remove temporary floor sections as the TPC installation progresses.

- 387 (o) Install sections of argon-distribution piping as the TPC installation pro-
388 gresses.
- 389 (p) Install the final end wall of vertical field cage at the access end of the cryostat.
390 These will be installed from the floor of the cryostat. Scaffolding will be
391 needed to install the supporting structure and then attach the panels to the
392 structure.
- 393 11. Remove movable scaffold and stair towers.
- 394 12. Temporarily seal the cryostat and test all channels for expected electronics noise.
- 395 13. Seal the access hatch.
- 396 14. Perform final test of all channels for expected electronics noise.

397 In general, APA panels will be installed in order starting with the panel furthest
398 from the hatch side of the cryostat and progressing back towards the hatch. The upper
399 field cage will be installed in stages as the installation of APA and CPAs progresses.
400 After the APAs are attached to the support rods the electrical connections will be made
401 to electrical cables that were already dressed to the support beams and electrical testing
402 will begin. Periodic electrical testing will continue to assure that nothing gets damaged
403 during the additional work around the installed APAs.

404 The TPC installation will be performed in three stages, each in a separate location;
405 the locations, or zones, are shown in Figure x-xx (this illustration was made for a 34-
406 kton, in-line underground detector, but the work zones are also applicable for the 10-
407 kton surface siting). First, in the clean room vestibule, a crew will move the APA and
408 CPA panels from storage racks, rotate to the vertical position and move them into the
409 cryostat. Secondly, in the panel-staging area immediately below the equipment hatch
410 of the cryostat, a second crew will transfer the lower panels from the crane to the
411 staging platform, connect the upper and lower panels together, route cables to the top
412 of stacked panels and finally transfer the stacked panels on to the monorail trolley that
413 moves within the cryostat. A third crew will reposition the movable scaffolding and use
414 the scaffold to make the mechanical and electrical connections at the top for each APA
415 and CPA as they are moved into position. The monorails inside and outside the cryostat
416 will each have two motorized trolleys so that work can be conducted by all three crews
417 in parallel. The steady-state rate for installation, given this work plan and a single-shift
418 schedule, is estimated to be two stacked panels per day.

419 The requirements for alignment and survey of the TPC are under development. Since
420 there will be plenty of cosmic rays in the surface detector and beam events, significant
421 corrections can be made for any misalignment of the TPC. The current plan includes
422 using a laser guide or optical transit and the adjustment features of the support rods
423 for the TPC to align the top edges of the APAs in the TPC to be straight, level and
424 parallel within a few mm. The alignment of the TPC in other dimensions will depend
425 on the internal connecting features of the TPC. The timing of the survey will depend
426 on understanding when during the installation process the hanging TPC elements are
427 in a dimensionally stable state. The required accuracy of the survey is not expected to
428 be finer than a few mm.

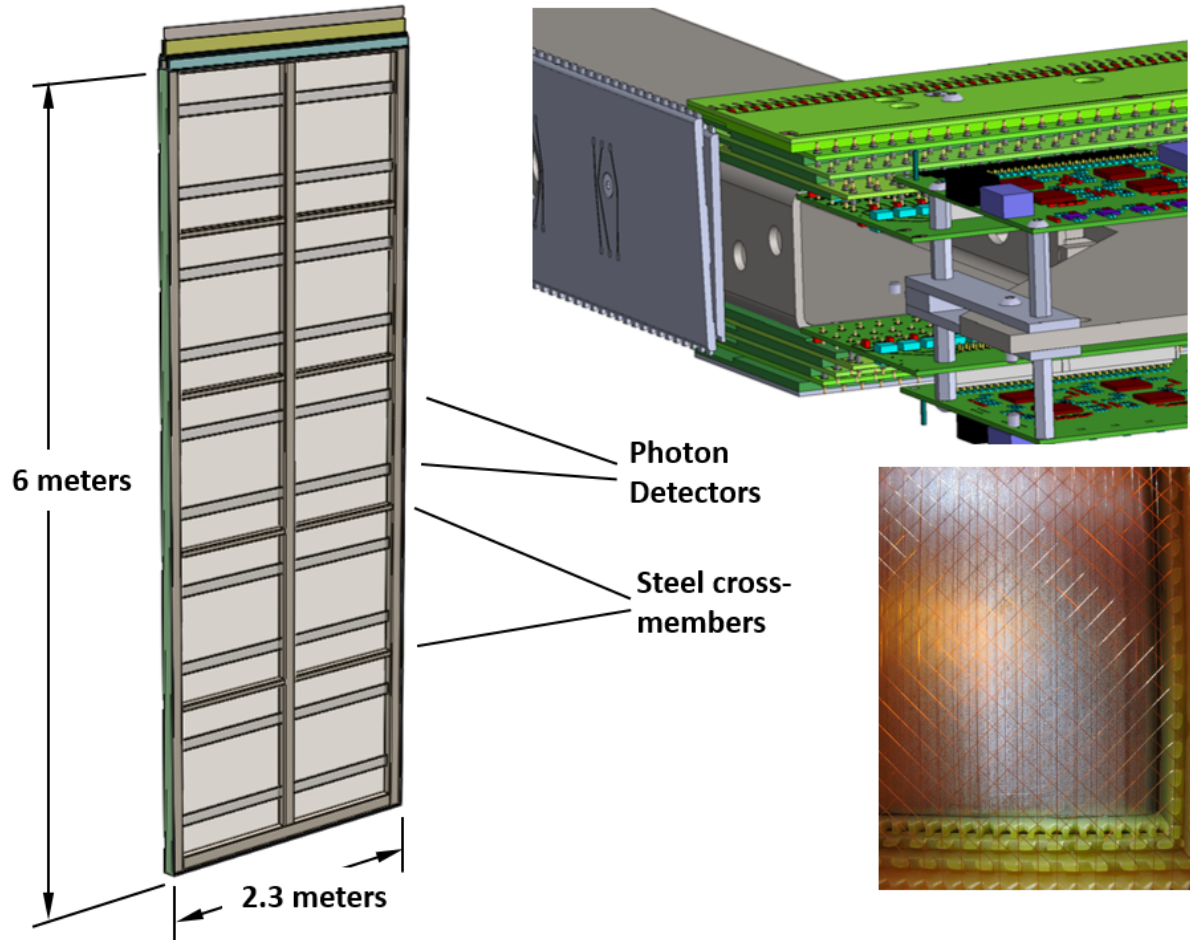


Figure 6: Clockwise from left: A full size APA, an APA corner showing the electronics boards, an APA lower corner photo showing wires and edge boards.

429 3.2.5 APA

430 The TPC consists of alternating anode plane assemblies (APAs) and cathode plane
431 assemblies (CPAs), with field-cage panels enclosing the four open sides between the
432 anode and cathode planes. A uniform electric field is created in the volume between
433 the anode and cathode planes. A charged particle traversing this volume leaves a trail
434 of ionization. The electrons drift toward the anode plane, which is constructed from
435 multiple layers of sense wires, inducing electric current signals in the front-end electronic
436 circuits connected to the wires.

437 The APAs are 2.3 m wide, 6 m long (plus an additional 0.3m of electronics), and 12
438 cm thick (Fig. 3.2.5). The 6 m length is a balance between maximizing the area per APA
439 and making them a practical length for fabrication, transportation and maneuvering into
440 final position in the TPC cryostat.

441 The 2.3 m width is chosen to fit in a standard HiCube shipping container for storage
442 and transport. The underlying structure of each APA is a framework of rectangular,
443 stainless steel tubing. The side and bottom edges of the frame are lined with multiple

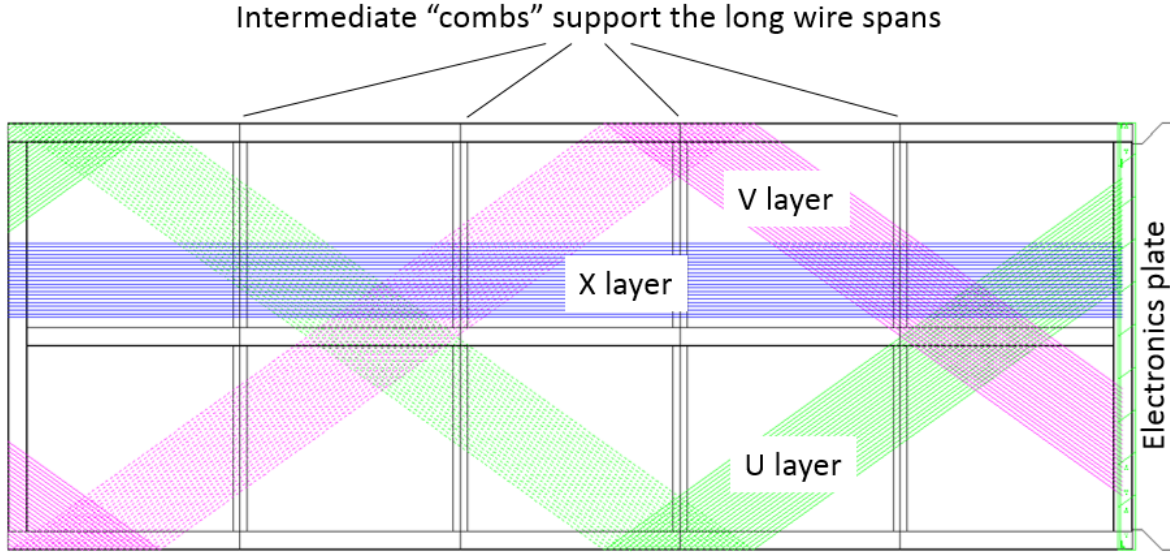


Figure 7: There are 3 instrumented layers of signal wires, one longitudinal and two angled, on each side of the APA which unambiguously locate an incident electron. The angled layers start at the electronics end and wind around to the other side on their way to the bottom. Partial layers are shown here; each layer fills the APA area completely. There is a fourth layer not shown (the G layer), above the instrumented layers that helps maintain the field.

444 layers of fiberglass circuit boards, notched along the edges to support and locate the
 445 wires that cross the APA face. The front-end electronics boards are mounted at the top
 446 end of the frame and protected by a metal enclosure.

447 Four planes of wires cover each side of the APA frame (Fig. 3.2.5). The inner three
 448 planes of wires are instrumented and are oriented, going from the inside out: longitudinally,
 449 and at $\pm 35.7\text{deg}$ to the long axis, respectively. Each wire is connected to a
 450 front-end readout channel. These three planes of sense wires provide redundancy against
 451 the occasional dead channel and ensure reliable 2D position reconstruction regardless
 452 of track angles. The wires on the outermost plane are oriented longitudinally. They
 453 shield the inner sense wires and are not connected to the readout electronics. With a
 454 wire pitches of 4.67 mm (diagonal layers) and 4.79 (straight layers), the total number of
 455 readout channels in an APA is 2560.

456 The distance between wire planes is 4.8 mm (3/16 in) corresponding with standard
 457 printed circuit board thickness, and while maintaining optimal signal formation. The
 458 four wire planes will be electrically biased so that electrons from an ionizing-particle
 459 track completely drift past the first three planes and are collected by the fourth plane.
 460 Calculations show that the minimum bias voltages needed to achieve this goal are V_G
 461 = -665V, V_U = -370V, V_V = 0V and V_X = 820V respectively (where G, U, V, and X
 462 are the wire-layer labels from outside in, towards the frame). It is convenient to set
 463 one of the wire planes to ground so that the wires can be DC coupled to the front-end
 464 readout electronics. In this instance, the V wire plane is set to ground potential to
 465 reduce the maximum bias voltages on the other wire planes, and enable the use of lower

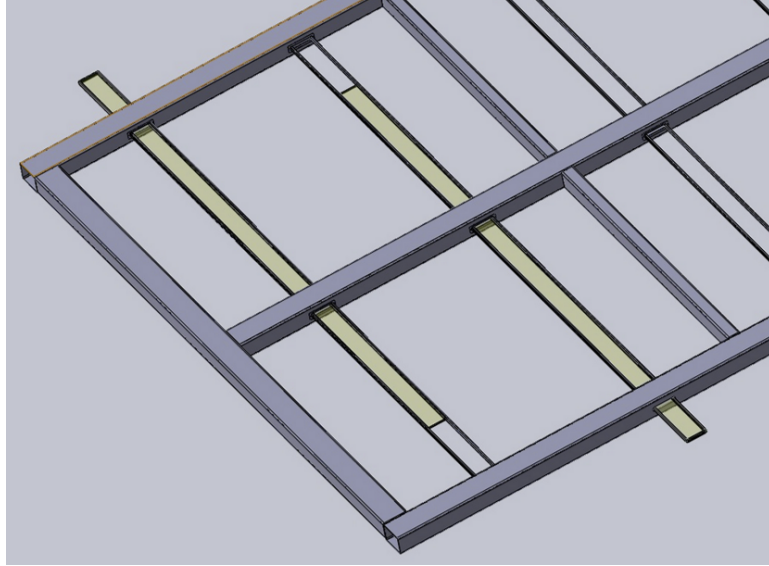


Figure 8: Photon detectors are mounted within the frame, between the wires on the two sets of four wire layers. The APA is built so that the photon detectors can be installed through slots in the side of the APA after the APA wires are installed. The wires that would cross these slots are routed around using copper traces on the edge boards.

466 voltage rated AC coupling capacitors. A grounded mesh plane, located 4.8 mm behind
 467 the collection (X) plane, prevents the electric field around this set of wires from being
 468 distorted by the metal frame structure and the wires on the opposite side of the frame. It
 469 also shields the sensing wires from potential EM interferences from the photon detectors
 470 (Fig. 3.2.5) mounted within the frame. The mesh should have a wire pitch less than 2
 471 mm to ensure a uniform electric field while maintaining a high optical transparency.

472 **3.2.6 CPA and Field Cage**

473 Each cathode plane (Fig. 9) is constructed from 6 identical CPA (cathode plane assem-
 474 bly) modules and two sets of end pieces. Each CPA is about half the size of an APA
 475 ($2.3\text{m} \times 3.1\text{m}$) for ease of assembly and transport. The CPA is made of a stainless-steel
 476 framework, with 4 pieces of thin FR4 sheets mounted in the openings. A receptacle for
 477 the HV feedthrough is attached to the upper corner of a cathode plane toward the roof
 478 entrance side to mate with the HV feedthrough in the cryostat ceiling.

479 The FR4 sheets on the CPAs are treated with layers of high resistive coating on both
 480 sides. The resistivity of the coating will be chosen such that the surface potential does
 481 not deviate significantly with the ionization current from the cosmic rays, and forms a
 482 relatively long time constant to dissipate the stored energy on each sheet in case of a
 483 high voltage discharge. This long RC time constant will also reduce the peak current
 484 injected into the front-end electronics in a HV discharge.

485 Due to the relatively high cosmic ray flux in this surface detector, it is preferable to
 486 prevent the scintillation light emitted by a cosmic ray between the cathode and cryostat
 487 wall from entering the TPC to reduce false trigger. The opaque cathode surface will
 488 service this purpose. The high flux of cosmic rays combined with very low drift velocity

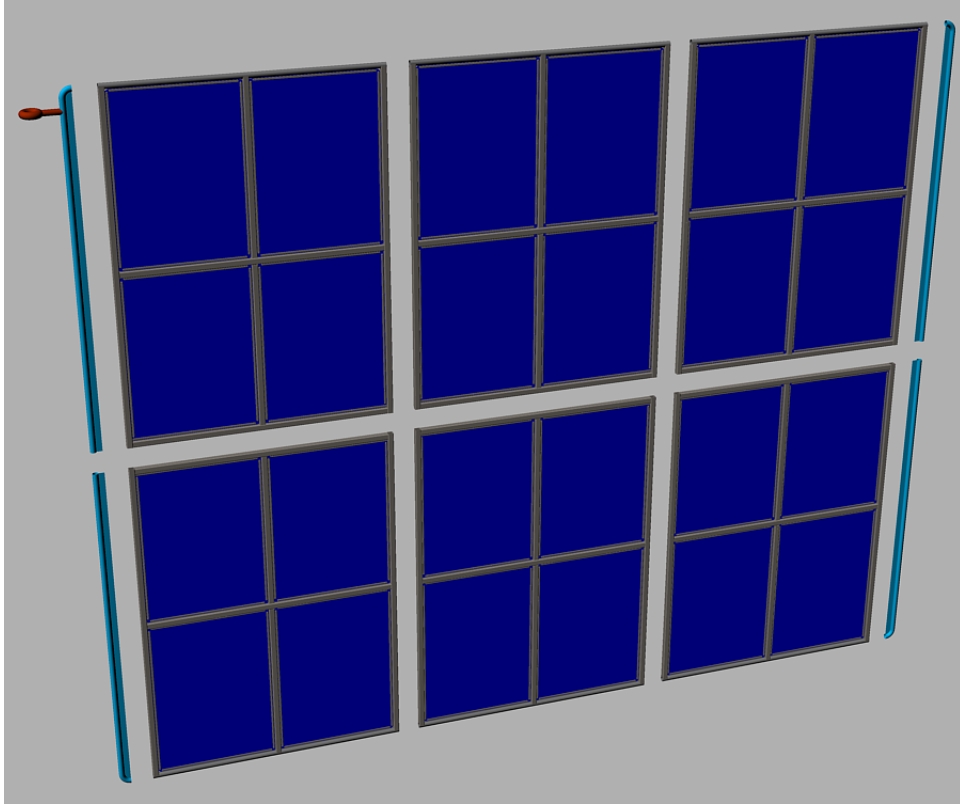


Figure 9: Exploded view of a cathode plane constructed from 6 CPA modules and 4 end pieces. The facing material on the CPA is highly resistive to minimize the peak energy transfer in case of a HV breakdown.

489 of positive ions in the liquid argon will result in sizable space charge distortions in
 490 the TPC (docdb #6471). In addition, the positive ions could build up further if the
 491 ion motion is slowed or stalled by counter flow in the LAr. Preliminary CFD analysis
 492 (docdb #6140) have shown that solid cathodes in the cryostat result in LAr flow pattern
 493 that neither causes excess positive ion buildup, nor degrades the LAr purity.

494 To achieve a 500 V/cm drift field over a 2.5 m distance, the bias voltage on the
 495 cathode plane must reach -125 kV. Two high voltage power supplies ($150 - 200$ kV) and
 496 two HV feedthroughs will be needed for the two cathode planes. The HV feedthroughs
 497 are based on the Icarus design, but modified to further improve their stability at higher
 498 voltages (Fig. 10).

Figure 10: Cross section of the HV feedthrough around the end of the grounded shield, and plot of the equi-potential contours between the HV central conductor and the ground shield. The flared end significantly reduces the electric field at the inside of the shield, improving HV stability.

499 Each pair of facing cathode and anode rows forms an electron-drift region. A field
 500 cage completely surrounds the four open sides of this region to provide the necessary
 501 boundary conditions to ensure a uniform electric field within, unaffected by the presence
 502 of the cryostat walls.



Figure 11: A section of the field cage in the 35ton TPC

503 The field cages are constructed using copper-clad FR4 sheets reinforced with fiber
 504 glass I-beams to form panels of $2.5\text{ m} \times 2.3\text{ m}$ in size for the top and bottom modules,
 505 and $2.5\text{ m} \times 2\text{ m}$ modules for the sides. Parallel copper strips are etched or machined
 506 on the FR4 sheets. Strips are biased at appropriate voltages through a resistive divider
 507 network. These strips will create a linear electric-potential gradient in the LAr, ensuring
 508 a uniform drift field in the TPC’s active volume.

509 Since the field cage completely encloses the TPC drift region on four (of six) sides,
 510 with the remaining two sides blocked by the solid cathodes, the FR4 sheets must be fre-
 511 quently perforated to allow natural convection of the liquid argon. The “transparency”
 512 of the perforation will be determined by a detailed LAr computerized fluid dynamic
 513 (CFD) study.

514 Figure 11 shows a section of the field cage in the 35ton TPC as it was being assembled.
 515 The 35ton TPC test results will inform us whether we should improve upon the current
 516 design, or change the design concept all together for this and future detectors. The main
 517 concern with the current field cage design is that the electric field at the edges of the
 518 copper strips is still quite high due to the thinness of the copper. One possible remedy is
 519 to cover the entire surface of the field cage with a high resistive coating. The resistivity
 520 between strips due to this coating must be kept many orders of magnitudes higher than
 521 the divider resistance to avoid distortion to the drift field. Fiigure 12 shows a FEA of
 522 such a configuration.

523 In the event of HV discharge on the cathode or the field cage, the voltage differential
 524 between neighboring field cage strips near the discharge electrode will be very high
 525 for a brief moment. This over voltage condition could cause damage to the field cage
 526 electrode and the resistors installed between strips. To minimize such disk, varistors or
 527 gas discharge tubes (GDT) will be installed between the field cage strips in parallel with
 528 the resistors to prevent excess voltage transient between the electrodes.

529 In order to test the installation concept of the far detector, the top and bottom field

530 cage modules will be attached to the mating CPAs through hinges. These combined
531 assembly will be installed into the cryostat and the field cage module opens to bridge
532 the CPA and the APA both mechanically and electrically.

533 3.2.7 TPC Readout

534 The TPC front-end (FE) electronics operate at cryogenic temperatures. The system
535 provides amplification, shaping, digitization, buffering and multiplexing of the signals.
536 The FE electronics consist of three boards stacked on top of one another: the Analog
537 Mother Board, the FPGA Mezzanine Board, and the SERDES Mezzanine Board. Figure
538 3.2.7 shows a schematic of the cold FE electronics.

539 The Analog Mother Board contains the front-end ASIC chips which perform the
540 analog readout of the TPC wires. The FE ASIC chip is implemented as a mixed-signal
541 ASIC providing amplification, shaping, digitization, buffering, a 16:2 multiplexing stage,
542 a driver and voltage regulators. The analog-to-digital converter on the ASIC samples
543 each TPC wire at 2 MHz. Eight such chips are mounted on a single readout board,
544 instrumenting 128 adjacent wires in one plane.

545 The two (multiplexed) signals from each FE ASIC are fed into the FPGA Mezzanine
546 Board. The cold FPGA aggregates the TPC data and also supplies the control and clock
547 to the FE ASICs. The FPGA on the mezzanine board receives the data and packages
548 the 128 channels together, one 2 MHz clock tick at a time. This is then sent to the
549 SERDES board for serialization and sent to the cryostat flange board over high-speed
550 (1 Gbps) serial links and finally to the DAQ system.

551 Besides the high-speed signal cable, which is a twin-axial cable bundle manufactured
552 by GORE, there are cable bundles for low-voltage power, wire-bias voltages, and various
553 slow controls and monitoring. Redundant cables will be provided for many of these
554 functions. The cable bundles will be connected through a feedthrough on the roof of the
555 cryostat.

parameter	value
ADC Sampling Rate	2 MHz
More stuff	
Cluster-on-Boards (COB)	3
Data-Processing-Modules (DPM)	12
ATCA Shelves	1 (6-slot)
TPC Readout Compute Nodes	3

557 The primary interface between the TPC front-end electronics (FE) and the DAQ sub-
558 system consists of an ATCA-based system of RCEs (Reconfigurable Cluster Elements).
559 The RCE system receives the serialized raw data for the FE, performs zero-suppression
560 on it, and packetizes and transmits the resulting sparsified data to a back-end data farm
561 for event building and further processing. Additionally, the RCE system transmits tim-
562 ing and control signals to the FE as well as forwarding configuration data to them at
563 start-up.

564 The RCE system consists the following components: a commercial ATCA shelf (2-,
565 6-, or 14-slot), a Cluster-On-Board (COB) which is the "front board" in ATCA terms,
566 and a Rear-Transition-Module (RTM) which is the "rear board". A schematic of the
567 system is shown in Figure 3.2.7. The COB is a custom board, developed by SLAC,

568 which holds the processing power of the system. The COB (see Figure ??) consists
569 of 5 bays for holding daughter boards, an onboard 10-GbE switch, and both 10- and
570 1-Gb ethernet connections for communications with the back-end system. Four of the
571 daughter-board bays are for Data Processing Modules (DPM), each of which can hold
572 up to two RCEs. The RCE is the core procession unit of the system; it is made up
573 of a modern SoC (currently, the Xilinx Zynq-7045) with multiple high-speed I/O ports
574 (up to 10-Gbps each) and external DRAM and flash memory controllers. The other bay
575 on the COB contains the Data Transmission Module (DTM) which is responsible for
576 distributing timing and trigger information to and between the DPMs.

577 While the COB hardware is application agnostic, the RTM is application specific.
578 The RTM provides the mechanical interface between the front-end (or, in our case, the
579 flange electronics) and the back-end, as well as other external sources such as the timing
580 or trigger systems. In this case we will use fiber optic connections between the flange
581 and the TPC DAQ using 8 12-channel (full duplex) CXP connectors on the RTM.

582 With the assumption that each cold FE board multiplexes it's 128 wire channels to 4
583 outputs at 1-Gbps each, the non-zero suppressed data for 1 APA can be fed into a single
584 COB (containing 8 RCEs). Each RCE would receive data from 2 FE boards, perform
585 zero-suppression, and send the result to the back-end.

586 MG***data rates?

587 3.2.8 Photon Detection System

588 3.3 Introduction

589 The ELBNF far detector will utilize liquid argon scintillation light to determine the
590 prompt event time of beam-driven and non-beam events. While the TPC will have far
591 superior spatial resolution to a photon detection system, the drift time for TPC events
592 is on the order of milliseconds. The beam clock will give much better timing resolution
593 than this but a photon detection system can determine the start of an event occurring
594 in the TPC volume (or entering the volume) to about 6 ns, which will be useful in
595 determining the t_0 of cosmic ray events, events from radiological decays, and corrections
596 to energy loss of the drifting electrons.

597 A charged particle passing through liquid argon will produce about 40,000 128 nm
598 photons per MeV of deposited energy. At higher fields this will be reduced due to
599 reduced recombination, but at 500 V/cm the yield is still about 20,000 photons per
600 MeV. Roughly 1/3 of the photons are prompt 2-6 ns and 2/3 are generated with a delay
601 of 1100-1600 ns. LAr is highly transparent to the 128 nm VUV photons with a Rayleigh
602 scattering length and absorption length of 95 cm and ≈ 200 cm respectively.

603 The relatively large light yield makes the scintillation process an excellent candidate
604 for determination of t_0 for non-beam related events. Detection of the scintillation light
605 may also be helpful in background rejection.

606 Several prototypes of photon detection systems have been developed by the LBNE,
607 now ELBNF, photon detector group over the past few years. There are currently three
608 prototypes under consideration for use in the ELBNF far detector, a baseline design along
609 with two alternate designs. A decision on the final design will be made in September
610 2015. The CERN neutrino platform ELBNF test would provide the first full scale test of

611 the ELBNF photon detector fully integrated into a full scale TPC anode plane assembly.

612 **3.4 Baseline Design (TPB-Coated Acrylic Bars)**

613 The reference design for the photon detection system is based on acrylic bars that are
614 200 cm long and 7.63 cm wide, which are coated with a layer of tetraphenyl-butadiene
615 (TPB). The wavelength shifter converts VUV (128 nm) scintillation photons striking it
616 to 430 nm photons inside the bar, with an efficiency of 50% of converting a VUV to
617 an optical photon. A fraction of the wavelength-shifted optical photons are internally
618 reflected to the bar's end where they are detected by SiPMs whose QE is well matched
619 to the 430 nm wavelength-shifted photons. All PD prototypes are currently using SensL
620 MicroFB-6K-35-SMT 6 mm ? 6 mm devices.

621 A full 6 m long APA will be divided into 5 bays with 2 PD modules (paddles)
622 instrumenting each bay (Fig. 1). The paddles will be inserted into the frames after the
623 TPC wires have been wrapped around the frames allowing final assembly at the CERN
624 test location. Two alternative designs are also under consideration.

625 **3.5 Alternate 1: Coated Acrylic Plate with Fiber Readout**

626 The first alternate design was motivated by a potential increase in the geometrical accep-
627 tance of the photon detectors. The number of required SiPMs and readout channels per
628 unit detector area covered with photon detection panels would be significantly reduced
629 to keep the overall cost for the photon detection system at or below the present design
630 while increasing the geometrical acceptance at the same time.

631 The prototype consists of a TPB-coated acrylic panel embedded with an S-shaped
632 wavelength shifting (WLS) fiber. The fiber is read out by two SiPMs, which are coupled
633 to either end of the fiber and serves to transport the light over long distances with
634 minimal attenuation. The double-ended fiber readout has the added benefit to provide
635 some position dependence to the light generation along the panel by comparing relative
636 signal sizes and arrival times in the two SiPMs. Figure 2 shows a schematic of the layout
637 and a picture of a prototype PD paddle.

638 **3.6 Alternate 2: Fiber Bundle with TPB-coated radiator**

639 Motivated by increasing the attenuation length of the PD paddles and allowing collection
640 of 400 nm photons coming from anywhere in the active volume of the TPC, the fiber-
641 bundle design utilizes a TPB-coated radiator situated in front of a bundle of wavelength-
642 shifting fibers (Fig. 3).

643 The fiber-bundle design is based on a thin TPB coated acrylic radiator located in
644 front of a close packed array of WLS fibers. This concept is designed so that roughly ?
645 of the photons converted in the radiator are incident on the bundle of fibers, which are
646 directed onto SiPMs at one end. The wavelength shifting fibers are Y11 UV/blue

647 from Kuraray and have mean absorption and emission wavelengths of about 440 nm
648 and 480 nm respectively. The attenuation length of the Y11 fibers is given to be greater
649 than 3.5 m at the mean emission wavelength, which will allow production of full-scale
650 (2 m length) photon detector paddles.

651 **3.7 Technology Selection**

652 The PD system tested at the CERN neutrino platform will be based on technology
653 selected later this year. The technology selection process will be based on a series of
654 tests planned for the next 6 months utilizing large research cryostats at Fermilab and
655 Colorado State University. The primary metric used for comparison between the three
656 technologies will be photon yield per unit cost. In addition to this metric PD threshold
657 and reliability will also serve as inputs to the final decision. A technical panel will be
658 assembled to make an unbiased decision.

659 Once the technology has been chosen the PD group will focus on optimizing the
660 selected design with the goal of procurement and assembly taking place in late FY 2016
661 and early FY 2016. The photon detector paddles will then be tested and shipped to
662 CERN in early FY 2017 for installation into the APAs in late FY 2017 in preparation
663 for installation into the test cryostat and operation in 2018.

664 **3.7.1 DAQ, Slow control and monitoring**

665 The DAQ will merge data to form events from the LArTPC, photon detector and beam
666 detector readouts using the artDAQ data acquisition toolkit using a farm of commercial
667 computers connected with an Ethernet switch. ArtDAQ is in use on several experiments
668 at Fermilab. We are using it on the 35t prototype, so we will have considerable experience
669 by the time of the CERN test.

670 The data collection for the CERN test will operate in a mode similar to that forseen
671 for the underground detectors. In order to collect data from non-beam interactions such
672 as proton decay candidates or atmospheric neutrinos, data will be continuously read in
673 to the artDAQ data receiver nodes and processed through the artDAQ system in quanta
674 corresponding to time intervals fixed from the time of the beginning of the run. These
675 are then transferred through the switch to a set of event building nodes which work in
676 parallel, each node receiving all the data from all the detectors for the time intervals it
677 is responsible for processing. There will be 32 parallel incoming data streams from the
678 LArTPCs and 16 streams from the photon detectors. There will be an additional stream
679 from the trigger board (the same board as built by Penn for the 35t test will be used)
680 which will receive input of the spill gate, warning of extraction, and pattern-unit bits
681 from trigger counters and other beamline instrumentation such as Cerenkov counters
682 [Which section are these described in?, should we refer to them from here?].

683 Synchronisation across all the input sources is essential in order that artDAQ can
684 bring together the data from the input streams correctly for processing by the event
685 building nodes. The data receiver nodes will provide overlap by repeating the data at
686 the boundaries of the time intervals so that a particle whose data spans two time intervals
687 can be collected. The time synchronisation is provided to the RTM back-module on the
688 LArTPC readout crates, to the SSP photon detector readout and to the trigger board
689 from a GPS based time synchrononisation distribution system originally designed for the
690 NOvA experiment. This system includes functionality to calibrate and correct for the
691 cable delays, and to send synchronisation control signals to the readout at predetermined
692 times.

693 The event building nodes will select time regions of interest within the time intervals
694 they are processing and form these into events to be written to disk. The algorithms

695 to select the events may be as simple as looking for a trigger bit in the trigger board
696 data stream, or may involve looking for self-triggered events in the LArTPC data. An
697 aggregation task, which is part of artDAQ will handle the parallelized event building
698 processes by merging the output events into a single stream and writing them to disk. To
699 avoid oversized output data files, when a predetrmined file size is reached, the aggregator
700 will switch to writing to a new file. The collaboraion requests to CERN, data links of
701 sufficient bandwidth to transfer these files from the CENF to the CERN data center,
702 and from there to locations worldwide for analysis.

703 Improved versions of the software systems which are being prototyped at the 35t test
704 will available for the CERN test including (a) Run control which controls and monitors
705 the DAQ processes and allows run starts and stops to be performed by the operator
706 (b) online monitoring (c) slow control of voltages and temperatures being used by the
707 electronics (this may not be comprehensive by the time of the CERN prototype, but we
708 plan on prototyping the readout of some of the quantities). The trigger board includes
709 facilities for generating calibration pulses and for identifying the event times of the
710 calibration events.

711 4 Cryostat and cryogenics system [~5 pages; **David/Barry/Jack**

712 Describe requirements to meet detector goals

713 4.1 LBNF detector

714 This section to provide context and illustrate which aspects need testing at the CERN
715 prototype

716 (Probably can take text from CDR once it's more developed)

717 4.2 CERN prototype detector

718 4.2.1 Cryostat from David Montanari

719 The Single Phase TPC test at CERN will use a membrane tank technology to contain
720 the base design of 725 tons of LAr equivalent to about $520m^3$. The design is based on
721 a scaled up version of the LBNE 35 Ton Prototype and the Fermilab Short Baseline
722 Near Detector. We propose that the cryostat be housed in the extension of the EHN1
723 Bat 887 at CERN, where the cryogenic system components will also be located. The
724 cryostat will use a steel outer supporting structure with a metal liner inside to isolate
725 the insulation volume, similar to the one of the dual phase detector prototype WA105
726 $1 \times 1 \times 3$ and to the Fermilab Short Baseline Near Detector. The support structure
727 will rest on I-beams to allow for air circulation underneath to maintain the temperature
728 within the allowable limits. The scope of the EHN1 cryostat subsystem includes the
729 design, procurement, fabrication, testing, delivery and oversight of a cryostat to contain
730 the liquid argon and the TPC. This section describes a reference design, whose scope
731 encompasses the following components:

- 732 • steel outer supporting structure,

- 733 • main body of the membrane cryostat (sides and floor),
734 • top cap of the membrane cryostat.

735 A membrane cryostat design commonly used for liquefied natural gas (LNG) storage
736 and transportation will be used. In this vessel a stainless steel membrane contains
737 the liquid cryogen. The pressure loading of the liquid cryogen is transmitted through
738 rigid foam insulation to the surrounding outer support structure, which provides external
739 support. The membrane is corrugated to provide strain relief resulting from temperature
740 related expansion and contraction. The vessel is completed with a top cap that uses the
741 same technology.

742 Two membrane cryostat vendors are known: GTT (Gaztransport & Technigaz) from
743 France and IHI (Ishikawajima-Harima Heavy Industries) from Japan. Each one is tech-
744 nically capable of delivering a membrane cryostat that meets the design requirements
745 for this detector. To provide clarity, only one vendor is represented in this document,
746 GTT; this is for informational purposes only. Figure 1 shows a 3D model of the GTT
747 membrane and insulation design.

748 The conceptual reference design for the Single Phase Test at CERN cryostat is a
749 rectangular vessel measuring 9.5 m in length (parallel to the beam direction), 7.3 m in
750 width, and 8.40 m in height; containing a total mass of 725 tons of liquid argon. Figure 18
751 shows side and end views of the cryostat respectively. Figure 3 shows a 3D view. To
752 minimize the contamination from warm surfaces, during operation the temperature of
753 all surfaces in the ullage shall be lower than 100 K. The top plate will contain two
754 hatches to install the TPCs and enter the tank, a manhole and several penetrations for
755 the cryogenic system and the detector.

756 **Design Parameters (from David Montanari)**

757 This design is meant to test technical solutions that may be of interest for future
758 needs of the Long Baseline Neutrino program. The use of a cold ullage (<100 K) to lower
759 the impurities in the gas region, and of a LAr pump outside the cryostat to minimize
760 the effect of noise, vibration and microphonics to the TPC inside the LAr are Value
761 Engineering studies for the Long Baseline program.

762 The design parameters for the TPC Test at CERN cryostat are listed in Table 3.

763 **Insulation system and secondary membrane (from David Montanari)**

764 The membrane cryostat requires insulation applied to all internal surfaces of the
765 outer support structure and roof in order to control the heat ingress and hence required
766 refrigeration heat load. The maximum required static heat leak is $15W/m^2$ for the floor
767 and the sides and $20W/m^2$ for the roof. Preliminary calculations show that it can be
768 obtained using 0.8 m thick insulation panels. Given an average thermal conductivity
769 coefficient for the insulation material of $0.0283 W/(m\cdot K)$, the heat input from the sur-
770 rounding steel is expected to be about 3.7 kW total. It assumes that the hatches are
771 foam insulated as well. This is shown in Table 4.

772 The insulation material is a solid reinforced polyurethane foam manufactured as
773 composite panels. The panels get laid out in a grid with 3 cm gaps between them
774 (that will be filled with fiberglass) and fixed onto anchor bolts anchored to the support
775 structure. The composite panels contain the two layers of insulation with the secondary
776 barrier in between. After positioning adjacent composite panels and filling the 3 cm
777 gap, the secondary membrane is spliced together by epoxying an additional overlapping

Table 3: Design requirements for the cryogenic system (has right values)

Design Parameter	Value
Type of structure	Membrane cryostat
Membrane material	SS 304/304L, 316/316L or equivalent. Other materials upon approval.
Outside reinforcement (support structure)	Steel enclosure with metal liner to isolate the outside from the insulation space, standing on legs to allow for air circulation underneath.
Total cryostat volume	583 m3
Total LAr volume	520 m3
LAr total mass	725,000 kg
Minimum inner dimensions (flat plate to flat plate).	7.3 m (W) x 9.5 m (L) x 8.4 m (H)
Depth of LAr	7.5 m (0.9 m ullage, same as LBNF)
Primary membrane	1.2 mm thick SS 304L corrugated stainless steel
Secondary barrier system	0.07 mm thick aluminum between fiberglass cloth. Overall thickness 1 mm located between insulation layers.
Insulation	Polyurethane foam (0.8 m thick from preliminary calculations)
Maximum static heat leak	15 W/m2
LAr temperature	88 +/- 1K
Operating gas pressure	Positive pressure. Nominally 70 mbarg (1 psig)
Vaccum	No vacuum
Design pressure	350 mbarg (5 psig) + LAr head (1,025 mbarg)
Design temperature	77 K (liquid nitrogen temperature for flexibility)
Temperature of all surfaces in the ullage during operation	
Leak tightness	<100 K
Maximum noise/vibration/microphonics inside the cryostat	LAr pump outside the cryostat
Beam window	In the center of the active volume. Precise location TBD.
Accessibility after operations	Capability to empty the cryostat in 30 days and access it in 60 days after the end of operations.
Lifetime / Thermal cycles	Consistent with liquid argon program. TBD.

778 layer of secondary membrane over the joint. All seams are covered so that the secondary
779 membrane is a continuous liner.

780 The secondary membrane is comprised of a thin aluminum sheet and fiberglass cloth.
781 The fiberglass- aluminum-fiberglass composite is very durable and flexible with an overall
782 thickness of about 1 mm. The secondary membrane is placed within the insulation space.
783 It surrounds the bottom and sides. In the unlikely event of an internal leak from the
784 primary membrane of the cryostat into the insulation space, it will prevent the liquid
785 cryogen from migrating all the way through to the steel support structure where it would
786 degrade the insulation thermal performance and could possibly cause excessive thermal
787 stress in the support structure. The liquid cryogen, in case of leakage through the inner
788 (primary) membrane will escape to the insulation volume, which is purged with GAr at
789 the rate of one volume exchange per day.

Table 4: Heat load calculation for the membrane cryostat (insulation thickness = 0.8 m). (note to self: has right values)

Element	Area (m^2)	K (W/mK)	ΔT (K)	Heat Input (W)
Base	83	0.0283	205	605
End walls	190	0.0283	205	1,374
Side walls	149	0.0283	205	1,081
Roof	83	0.0283	205	605
Total				3,665

790 Cryostat Configuration (from David Montanari)

791 This section describes the configuration of the cryostat only. The TPC is described
792 in Section xxx. With the intent to minimize the contamination in the gas region, the
793 ullage will be kept cold (<100 K). A possible way to achieve this requirement is to spray
794 a mist of clean liquid and gaseous argon to the metal surfaces in the ullage and keep
795 them cold, similar to the strategy that was developed for the cool down of the LBNE 35
796 Ton prototype.

797 Outer Support Structure (from David Montanari)

798 The reference design is a steel support structure with a metal liner on the inside
799 to isolate the insulation region and keep the moisture out. This choice allows natural
800 and forced ventilation to maintain the temperature of the steel within acceptable limits,
801 without the need of heating elements and temperature sensors. It reduces the time
802 needed for the construction: the structure will be prefabricated in pieces of dimensions
803 appropriate for transportation, shipped to the destination and only assembled in place.
804 Fabrication will take place at the vendor's facility for the most part. This shortens the
805 construction of the outer structure on the detector site, leaving more time for completion
806 of the building infrastructure. If properly designed, a steel structure may allow the
807 cryostat to be moved, should that be desired later in the future.

808 Main body of the membrane cryostat (from David Montanari)

809 The sides and bottom of the vessel constitute the main body of the membrane cryo-
810 stat. They consist of several layers. From the inside to the outside the layers are stainless

811 steel primary membrane, insulation, thin aluminum secondary membrane, more insula-
812 tion, and steel outer support structure with metal panels acting as vapor barrier. The
813 secondary membrane contains the LAr in case of any primary membrane leaks and
814 the vapor barrier prevents water ingress into the insulation. The main body does not
815 have side openings for construction. The access is only from the top. There is a side
816 penetration for the liquid argon pump for the purification of the cryogen.

817 **Top cap (from David Montanari)**

818 Several steel reinforced plates welded together constitute the top cap. The stainless
819 steel primary membrane, intermediate insulation layers and vapor barrier continue across
820 the top of the detector, providing a leak tight seal. The secondary barrier is not used nor
821 required at the top. The cryostat roof is a removable steel truss structure that bridges
822 the detector. Stiffened steel plates are welded to the underside of the truss to form a flat
823 vapor barrier surface onto which the roof insulation attaches directly. The penetrations
824 will be clustered in the back region, as far away from the beam as possible. The top cap
825 will have a large opening for TPC installation, a secondary smaller opening for personnel
826 access and a manhole.

827 The truss structure rests on the top of the supporting structure where a positive
828 structural connection between the two is made to resist the upward force caused by the
829 slightly pressurized argon in the ullage space. The hydrostatic load of the LAr in the
830 cryostat is carried by the floor and the sidewalls. Everything else within the cryostat
831 (TPC planes, electronics, sensors, cryogenic and gas plumbing connections) is supported
832 by the steel plates under the truss structure. All piping and electrical penetration into
833 the interior of the cryostat are made through this top plate, primarily in the region of
834 the penetrations to minimize the potential for leaks. Studs are welded to the underside
835 of the top plate to bolt the insulation panels. Insulation plugs are inserted into the
836 bolt-access holes after panels are mounted. The primary membrane panels are first
837 tack-welded then fully welded to complete the inner cryostat volume.

838 Table 5 presents the list of the design parameters for the top of the cryostat.

839 **Cryostat grounding and isolation requirements (from David Montanari)**

840 The cryostat has to be grounded and electrically isolated from the building. This
841 section presents the list of the current grounding and isolation requirements for the
842 cryostat. Figure 19 shows the layout of the top plate grounding.

843 **Isolation**

- 844 1. The cryostat membrane and any supporting structure, whether it is a steel struc-
845 ture or a concrete and rebar pour, shall be isolated from any building metal or
846 building rebar with a DC impedance greater than 300 kΩ.
- 847 2. All conductive piping penetrations through the cryostat shall have dielectric breaks
848 prior to entering the cryostat and the top plate.

849 **Grounding**

- 850 1. The cryostat, or “detector” ground, shall be separated from the “building” ground.
- 851 2. A safety ground network consisting of saturated inductors shall be used between
852 detector ground and building ground.

Table 5: Design parameters for the cryostat top (has right values)

Design Parameter	Value
Configuration	Removable metal plate reinforced with trusses anchored to the membrane cryostat support structure. Contains multiple penetrations of various sizes and a manhole. Number, location and size of the penetrations TBD. Provisions shall be made to allow for removal and re-welding six (6) times.
Plate/Trusses non-wet material	Steel if room temperature. SS 304/304 or equivalent if at cryogenic temperature
Wet material	SS 304/304L, 316/316L or equivalent. Other materials upon approval.
Fluid	Liquid argon (LAr)
Design pressure	350 mbarg (5 psig)
Design temperature	77 K (liquid nitrogen temperature for flexibility)
Inner dimensions	To match the cryostat
Maximum allowable roof deflection	0.028 m (span/360 from LBNF)
Maximum static heat leak	<20 W/m ²
Temperatures of all surfaces in the ullage during operation	<100 K
Additional design loads	<ul style="list-style-type: none"> - Top self-weight - TPC (3,000 kg on each anchor) - TPC anchors (TBD) - Live load (488 kg/m²) - Electronics racks (400 kg in the vicinity of the feed through) - Services (150 kg on every feed through)
TPC anchors	Capacity: 3,000 kg each anchor. Number and location TBD. Minimum 6.
Hatch opening for TPC installation	3,550 m x 2,000 m (location TBD)
Grounding plate	1.6 mm thick copper sheet brazed to the bottom of the top plate
Lifting fixtures	Appropriate for positioning the top at the different parts that constitute it.
Cold penetrations	Minimum 4 (??). Location and design TBD.
Lifetime / Thermal cycles	Consistent with the liquid argon program TBD.

853 3. Parameters TBD.

854 **Top plate grounding**

- 855 1. If the cryostat is contained within a concrete pour, the top plate shall be electrically
856 connected to any rebar used in that pour, and the rebar shall be conductively tied
857 at regular intervals. Parameters TBD.
- 858 2. The top grounding plate shall be electrically connected to the cryostat membrane
859 by means of copper braid connections.
 - 860 (a) Each connection shall be at least 1.6 mm thick and 63.5 mm wide.
 - 861 (b) The length of each connection is required to be as short as possible.
 - 862 (c) The distance between one connection and the next one shall be no more than
863 1.25 m.
 - 864 (d) The layout can follow the profile of several pieces of insulation, but it shall
865 be continuous.
 - 866 (e) The DC impedance of the membrane to the top plate shall be less than 1
867 ohm.

868 **Leak prevention (from David Montanari)**

869 The primary membrane will be subjected to several leak tests and weld remediation,
870 as necessary. All (100%) of the welds will be tested by an Ammonia colorimetric leak
871 test (ASTM E1066-95) in which welds are painted with a reactive yellow paint before
872 injecting a Nitrogen-Ammonia mixture into the insulation space of the tank. Wherever
873 the paint turns purple or blue, a leak is present. The developer is removed, the weld
874 fixed and the test is performed another time. Any and all leaks will be repaired. The
875 test lasts a minimum of 20 hours and is sensitive enough to detect defects down to
876 0.003 mm in size and to a $10^{-7} \text{ std } - \text{cm}^3/\text{s}$ leak rate (equivalent leak rate at standard
877 pressure and temperature, 1 bar and 273 K). To prevent infiltration of water vapor
878 or oxygen through microscopic membrane leaks (below detection level) the insulation
879 spaces will be continuously purged with gaseous argon to provide one volume exchange
880 per day. The insulation space will be maintained at 30 mbar, slightly above atmospheric
881 pressure. This space will be monitored for changes that might indicate a leak from the
882 primary membrane. Pressure control devices and safety relief valves will be installed on
883 the insulation space to ensure that the pressure does not exceed the operating pressure
884 inside the tank. The purge gas will be recirculated by a blower, purified, and reused as
885 purge gas. The purge system is not safety- critical; an outage of the purge blower would
886 have negligible impact on LAr purity.

887 **Cryostat size from TPC dimensions (from Jack Fowler)**

888 The minimum internal size of the cryostat is determined from size of the TPC. At the
889 bottom of the cryostat there needs to be a minimum of 0.3 m between the frame of the
890 CPA and closest point on the SS membrane. This is to prevent high voltage discharge
891 between the CPA and the electrically grounded membrane. It is foreseen that there
892 would be some cryogenic piping and instrumentation under the TPC. There is a height
893 allowance of 0.1 m for this. There will be access and egress space around the outside of

894 the TPC and the membrane walls. On three sides, 1.0 m of space is reserved for this.
895 The final side of the TPC will have piping and instrumentation for the cryogenic system.
896 There will be 1.3 m of space reserved for this.

897 The support system for the TPC will be located at the top between the underside
898 of the cryostat roof and the top of the TPC. The plan is to model this space similar to
899 what is planned for the far site TPC. There will be 0.9 m of ullage space. In order to
900 prevent high voltage discharge, the upper most part of the CPA needs to be submerged a
901 minimum of 0.3 m below the liquid Argon surface. The top of the TPC will be separated
902 from the membrane by a minimum of 1.2 m.

903 Adding all of these to the size of the TPC yields the minimum inner dimensions of
904 the cryostat. A minimally sized cryostat would be 9.5 m long, 7.3 m wide and 8.4 m
905 high. This assumes the TPC will be positioned inside the cryostat with the CPAs and
906 end field cages parallel to the walls of the cryostat. Also there is no space allotted for
907 a beam window to enter the cryostat. Clearance would need to be added if it violates
908 any of the current boundaries listed above. These dimensions also preserve the ability
909 to reverse the order of the APAs and CPAs inside the TPC. The current plan is to have
910 the APAs located in the center of the cryostat with a CPA on each side. Reversing this
911 to have the CPA in the center and APAs on each side may be required to achieve some
912 of the proposed physics. The orientation of the TPC components will be finalized after
913 various scenarios have been sufficiently simulated.

914 4.3 Cryogenic System (from David Montanari)

915 The cryogenic system is being developed as part of the international engineering team
916 set up between Fermilab and CERN to design, fabricate and install cryogenic systems
917 of similar requirements and increased size for Short and Long Baseline at Fermilab, and
918 WA105s at CERN. The goal is to develop a single model and adapt if for all future
919 generation detectors, with the necessary scaling up in size and adjustments for eventual
920 different needs of the different detectors. Table 6 presents the list of requirements for
921 the cryogenic system for the Single Phase TPC test at CERN detector.

922 Figure 20 outlines the basic scheme of the LN2 supply system, which was proposed
923 by CERN for the Short Baseline Program and agreed as an appropriate solution for
924 this detector as well. The experiment will rely on LN2 tankers for regular deliveries to a
925 local dewar storage, which will be sized to provide several days of cooling capacity in the
926 event of a delivery interruption. From the dewar storage the LN2 is then transferred to
927 a distribution facility located in the experimental hall. It includes a small buffer volume
928 and an LN2 pumping station that transfers the LN2 to the argon condenser and other
929 services as needed. The low estimated heat leak of the vessel (3.5 kW) and the location
930 inside an above ground building allow for use of an open loop system typical of other
931 installations operated at Fermilab (LAPD, LBNE 35 ton prototype, MicroBooNE) and
932 at CERN (???). Main goal of the LN2 system is to provide cooling power for the argon
933 condenser, the initial cool down of the vessel and the detector, and all other services as
934 needed.

935 Figure 21 shows a schematic diagram of the proposed liquid argon system. It is based
936 on the design of the LBNE 35 ton prototype, the MicroBooNE detector systems and the
937 current plans for the Long Baseline Far Detector.

938 Main goal of the LAr system is to purge the tank prior to the start of the operations
 939 (with GAr in open and closed loop), cool down the tank and fill it with LAr. Then con-
 940 tinuously purify the LAr and the boil off GAr to maintain the required purity (electron
 941 lifetime measured by the detector).

942 The LAr receiving facility includes a storage dewar and an ambient vaporizer do
 943 deliver LAr and GAr to the cryostat. The LAr goes through the liquid argon handling
 944 and purification system, whereas the Gar through the gaseous argon purification before
 945 entering the vessel. The LAr purification system is currently equipped with a filter
 946 containing mol sieve and copper beds, and a regeneration loop to regenerate the filter
 947 itself. The filter medium may change following the ongoing developments on filtration
 948 schemes, but the concept remains the same.

949 During operation, an external LAr pump circulates the bulk of the cryogen through
 950 the LAr purification system. The boil off gas is first re-condensed and then is sent to
 951 the LAr purification system before re-entering the vessel.

Table 6: Design requirements for the cryogenic system

Parameter	Value
Location	Preferably not in front of the cryostat (on the beam)
Cooling Power	TBD based on the heat leak of the cryostat (estimated 3.5 kW), the cryo-piping and all other contributions (cryogenic pumps, etc.)
Liquid argon purity in cryostat	10 ms electron lifetime (30 ppt O ₂ equivalent)
Gaseous argon piston purge rate of rise	1.2 m/hr
Membrane cool-down rate	From manufacturer
TPCs cool-down rate	<40 K/hr, <10 K/m (vertically)
Mechanical load on TPC	The LAr or the gas pressure shall not apply a mechanical load to the TPC greater than 200 Pascal.
Nominal LAr purification flow rate (filling/ops)	5.5 day/volume change
Temperature of all surfaces in the ullage during operations	<100 K
Gaseous argon purge within insulation	1 volume change /day of the open space between insulation panels.
Lifetime of the cryogenic system	Consistent with the LAr program. TBD.

952 **5 Charged Particle Test Beam Requirements [~ 10
 953 pages; Cheng-Ju]**

954 **5.1 Particle Beam Requirements**

955 The requested beam parameters are driven by the requirement that the results from the
 956 CERN test beam should be directly applicable to the future large underground single-
 957 phase LAr detector with minimal extrapolation. The CERN test beam data will be
 958 used to evaluate the detector performance, to understand the various physics systematic
 959 effects, and to provide “neutrino-like” data for event reconstruction studies. The chosen
 960 beam parameters span a broad range of particle spectrum that are expected in the future
 961 neutrino experiment. The particle beam composition should consist of electrons, muons,
 962 and hadron beams that are charge-selected. The particle momentum of interest ranges
 963 from 0.2 GeV/c to 10 GeV/c. The maximum electron drift time in the TPC is about
 964 3 ms. To minimize pile-up in the TPC, the desired beam rate should be around 200
 965 Hz with the maximum rate below 300 Hz. The single-phase TPC consists of two drift
 966 volumes. It is desirable to aim the particle beam so that hadronic showers are mostly
 967 contained in the same drift volume. However, we also plan to take some data with
 968 hadronic shower crossing the midplane of the TPC from one drift volume to another.
 969 The two beam entry angles and positions with respect to the LAr cryostat are illustrated
 970 in Figure [XYZ.] The summary of the beam requirements are shown in Table 7.

Table 7: Particle beam requirements.

Parameter	Requirements	Notes
Particle Types	e^\pm, μ^\pm, π^\pm	
Momentum Range	0.2 - 10 GeV/c	
Momentum Spread	$\Delta p/p < 5\%$	
Transverse Beam Size	RMS(x,y) < 2.5 cm	At the entrance face of the LAr cryostat
Beam Divergence		
Beam Angle	$\approx 20^\circ$	
Beam Dip Angle	-6° (nominal); $\pm 5^\circ$ range	
Beam Entrance Position		
Rates	200 Hz (average); 300 Hz (maximum)	

971 **5.2 EHN1 H4ext Beamline**

972 The H4ext is an extension of the existing H4 beamline in Experimental Hall North 1
 973 (EHN1). To produce particles in the momentum range of interest, 60 - 80 GeV/c pion
 974 beam from the T2 target is used to generate tertiary beams. The tertiary particles are
 975 momentum and charge-selected and transported down H4ext beamline to the experi-
 976 mental area. A preliminary layout of the H4ext beamline is shown in Figure 22.

977 **5.2.1 Beam Optics**

978 [Waiting for inputs from Ilias]

979 **5.2.2 Expected Rates and Purity**

980 [Waiting for inputs from Ilias]

981 **5.3 Beam Instrumentation**

982 **5.3.1 Beam Position Detector**

983 **5.3.2 Time-of-Flight Detector**

984 **5.3.3 Threshold Cherenkov Counter**

985 **5.4 Muon Beam Halo Counters**

986 The halo counter is a set of plastic scintillator paddles surrounding the beamline. The
987 main purpose is to tag particles (primarily muons from the upstream production target)
988 that are outside of the beam axis, but may potentially enter the TPC volume. The
989 counter information is used to either veto or simply flag these class of events.

990 **5.5 Beam Window on LAr Cryostat**

991 This section could be absorbed into the cryostat chapter.

992 **6 Computing requirements, data handling and soft-**
993 **ware [~ 3 pages; Maxim Potekhin/Craig Tull]**

994 **6.1 Overview**

995 The proposed “Full Scale” test of a single-phase Liquid Argon TPC at CERN, performed
996 in the context of the WA105 project and its evolution, will build upon the technology and
997 expertise developed in the process of design and operation of its smaller predecessor, the
998 35t detector at FNAL. This includes elements of front-end electronics, data acquisition,
999 run controls and related systems. We also expect that for the most part, Monte Carlo
1000 studies necessary to support this program will be conducted utilizing software evolved
1001 from tools currently used (2015).

1002 In the test-beam setup, the detector performance will be characterized for different
1003 types of particles, e.g. p , π^\pm , μ^\pm etc. Current plans call for measurements in pre-defined
1004 bins of the incident particle momentum, which will have widths ranging from tens to
1005 hunderds of MeV (see 6.2.4). The volume of data to be recorded shall be determined by
1006 the number of events that need to be collected in each measurements that provides
1007 adequately low statistical uncertainty of the parameters measured.

1008 In our view, it is optimal to first stage the “precious” data collected from the proto-
1009 type on disk at CERN and then sink it to tape (also at CERN), while simultaneously
1010 performing replication to data centers in the US. For the latter, FNAL is the prime

1011 candidate, with additional data centers at Brookhaven National Laboratory and the
1012 NERSC facility as useful additional locations for better redundancy and more efficient
1013 access to the data from greater number of locations.

1014 6.2 Collecting and Storing Raw Data

1015 6.2.1 Executive Summary

1016 As we will show in subsequent sections, the total amount of data to be collected during
1017 the prototype operation will be considerable under all assumptions and estimates. To
1018 fulfill the mission of this test beam experiment, we expect that we will need tape storage
1019 of $O(PB)$ size, and a more modest disk space for raw data staging at CERN, for repli-
1020 cation purposes. There will be additional requirements for processed and Monte Carlo
1021 data placement which we expect to be mostly done in the US (but not exclusively).

1022 6.2.2 Event Size Estimates

1023 In addition to the principal sensitive volume where Liquid Argon will serve as active
1024 medium, the prototype will also contain a Photon Detector designed to record light
1025 pulses produced in Argon due to scintillation caused by ionizing radiation. In any
1026 realistic scenario, the amount of data to be produced by the Photon Detector will be
1027 quite small compared to that of the Liquid Argon TPC. Same goes for other elements
1028 of the experimental apparatus (hodoscopes, trigger systems etc) and as a result, for the
1029 purposes of this section, we wil focus only on the Liquid Argon TPC as the critical and
1030 massive source of data.

1031 At the time of writing, work is being done on determination of the physical design of
1032 the Liquid Argon prototype, and the number of the Anode Plane Assemblies (APA) to
1033 be included in the detector is not yet finalized (e.g. 3 vs 6). There is therefore at least a
1034 factor of two uncertainty in the number of readout channels in the detector (e.g. 7680 vs
1035 15360). This would affect the amount of data produces by DAQ (although not necessarily
1036 by a factor of two since a large part of the raw data will be zero-suppressed and occupancy
1037 in general is expected to be low), and there will be additional tracks (or track segments)
1038 produced by cosmic ray muons. From the two channel count numbers quoted above, we
1039 assume the smaller number of channels for the purposes of this discussion.

1040 Some estimates for the scale of the data representing a charged track in the 0.5-10.0
1041 GeV range (which is characteristic of the CERN test being planned) can be made based
1042 on existing earlier calculations for the beam neutrino events as they would appear in
1043 the LBNE Far Detector. For this we assume digitization rate fixed at 2MHz, and 4312
1044 samples per drift window. The theoretical **upper limit** on the number of channels
1045 above the threshold of zero-suppression will be approximately of the order of channel
1046 count in a single APA, i.e. around 2500. Since each sample is 16 bit (12 bit is the more
1047 recent number), we arrive to the limit of approximately 20MB per single charged track.
1048 For this class of events, the amount of data will scale roughly linearly with the length
1049 of the track (cf. cases when a track is stopped or leaves the sensitive volume).

1050 In most cases the data will be zero-suppressed at the source. The data reduction
1051 factor will depend on a variety of parameters, but as a rule of thumb it's an order of

1052 magnitude. We conclude therefore that we will have events of typical size of a few
1053 megabyte. We present quantitative estimates in 6.2.4.

1054 6.2.3 “Before” and “After” Readout Windows

1055 According to various estimates, given the volume of the LAr prototype, we can expect
1056 $O(1)$ cosmic ray tracks to overlay the triggered “beam” events. This leads to extra data
1057 included in each event by a value commensurate with single muons.

1058 In addition to increasing the size of each nominal beam event, there is another conse-
1059 quence of this type of background. Since one of the principal goals of this experiment is
1060 to create a data sample which will allow us to precisely characterize and improve track-
1061 ing and pattern recognition algorithms of a realistic detector, there must be ways to
1062 distinguish signals due to the incident beam particle vs various sources of background,
1063 of which most important is the cosmic ray background. Since overlay of cosmic ray
1064 muons over beam events is stochastic in nature, we need to make an effort to record
1065 those signals which were produced “just before” and “just after” the arrival of the test
1066 particle from the beamline, and thus be able to account for partial background tracks
1067 in the main event, with a high degree of certainty. Since the natural time scale of the
1068 detector is the total drift time for the collection volume, this leads to the requirement
1069 that we record three time windows instead of one. For the purposes of the data vol-
1070 ume bookkeeping, this translated into adding three muon tracks worth of data, to the
1071 nominal event.

1072 6.2.4 Statistics and the Volume of Data

1073 Experimental program for the test includes triggering on a few types of particles over
1074 a range of momenta. We introduce bins for the particle momenta as shown in the
1075 table below. The estimated event sizes listed in the table are based on Monte Carlo
1076 studies performed earlier for the 10kt version of the LBNE Far Detector. Hadronic and
1077 electromagnetic showers were included in these estimates. As a concrete example, for
1078 an incident electron of 4GeV/c momentum calculations indicate an average event size
1079 of $\sim 2\text{MB}$, after zero-suppression.

Particle Type	Momentum Range (GeV/c)	Bin (MeV/c)	Approx. event size, MB	Approx. # of events, 10^6
p	0.1-2.0	100	1	1
p	2.0-10.0	200	5	1
μ^\pm	0.1-1.0	50	1	1
μ^\pm	1.0-10.0	200	5	1
e^\pm	0.1-2.0	100	1	1
e^\pm	2.0-10.0	200	4	1
K^+	0.1-1.0	100	1	1
$\gamma(\pi^0)$	0.1-2.0	100	1	1
$\gamma(\pi^0)$	2.0-5.0	200	5	1

1081 Preliminary plans call for statistics of the order of $10^5 - 10^6$ events to be collected in
1082 each bin, so in the table above we marked it as nominal 1M events for each entry. The
1083 requirements to the scale of these statistics are currently being refined.

1084 Depending on the assumptions, this translates into \sim 220 million events total (for all
1085 event classes) to ensure enough statistics for subsequent analysis. Utilizing a spreadsheet
1086 model, and taking into account the cosmic ray overlay and additional readout windows
1087 as explained in 6.2.3, we arrive to a number of \sim 3PB for total storage space necessary
1088 to host **the raw data**. This needs to be looked at as the basis for tape budget. As
1089 explained below, this volume of data needs to be replicated for assured preservation, in
1090 at least one more additional facility, hence in effect this number must be doubled when
1091 budgeting tape.

1092 **6.2.5 Data Acquisition and Storage**

1093 The Data Acquisition System used in this experiment will be derived from the system
1094 currently used in the 35t Liquid Argon prototype being commissioned at FNAL. We
1095 foresee three Linux workstations equipped with interface cards to be used for data read-
1096 out. It will be necessary to provide a stage-out disk space (a few tens of TB in size) to
1097 serve as a buffer for the DAQ system, from which the data will be transmitted to

- 1098 • Tape storage at CERN.
- 1099 • Storage facility at Fermilab, where the data will be written to tape and also staged
1100 in dCache as necessary for express analysis.
- 1101 • *Optional* other locations, such as auxiliary storage at Brookhaven National Lab-
1102 oratory , which is now being planned according to the data volumes estimated in
1103 this paper. NERSC facility has considerable potential in serving as an additional
1104 data hub. Partial copies will be transmitted to other National Laboratories and
1105 research centers.

1106 Considerable volume of the raw data makes unlikely that it will be all staged on disk
1107 at any single location, in its entirety. We foresee the need for ample amount of tape
1108 storage, and a smaller disk space (\sim 0.5-1.0PB) for staging raw data coming out of the
1109 detector - in transit to tape storage and CERN and the US facilities.

1110 **6.2.6 Raw Data Transmission and Distribution**

1111 As mentioned in 6.2.5, at least two full replicas will exist for the raw data - at CERN
1112 and at FNAL (and likely an additional replica at BNL). Moving data outside CERN is
1113 subject to a number of requirements that include:

- 1114 • automation
- 1115 • monitoring
- 1116 • error checking and recovery (redundant checks to ensure the “precious” data was
1117 successfully sunk to mass storage at the endpoint)
- 1118 • compatibility with lower-level protocols that are widespread, well understood and
1119 maintained (cf. gridFTP)

1120 There are a number of systems that can satisfy these requirements, and one of them
1121 where we possess sufficient expertise and experience is Spade, first used in IceCube [1]
1122 and then enhanced and successfully utilized in Daya Bay experiment [2].

1123 Note that at this stage of the lifecycle of the data we foresee transmission between
1124 fixed endpoints (with sufficient degree of automation, checking, redundancy etc) but
1125 we haven't discussed yet the topic of how such data is made available to researchers
1126 who wish process it at their home institution or on the Grid/in the Cloud - this will be
1127 addressed in 6.5.

1128 **6.3 Databases**

1129 A few types of databases will be required:

- 1130 • Run Log, Conditions and Slow Controls records
- 1131 • Offline Calibrations

1132 Databases listed in the former item will need to be local to the experiment in order
1133 to reduce latency, improve reliability, reduce downtime due to network outages etc. A
1134 replication mechanism will need to be put in place the data is readily available at the
1135 US and other sites. The volume of data stored in these databases will likely to be quite
1136 modest.

1137 As to the offline calibrations, for optimal access, such databases should be located
1138 closer to the location where most processing will take place. FNAL is a good candidate
1139 for that (also from the support point of view), and we shall also consider replication of
1140 these database to other research institutions.

1141 **6.4 A note on Simulation and Reconstruction Software**

1142 Research effort connected to the “Full Scale” prototype at CERN will benefit from
1143 utilizing simulation toolkits, and tracking and other reconstruction algorithms created
1144 by communities such as former LBNE, and especially during the 35t test at FNAL. In
1145 order to leverage this software and expertise, appropriate manpower will need to be
1146 allocated in order to create and maintain physics analysis tools necessary to fulfill the
1147 research goals of this experiment.

1148 These tools will rely on software components which will need to be portable, well
1149 maintained and validated, given the widely distributed nature of the Collaboration and
1150 the need to use geographically dispersed resources. To ensure that this happens, we
1151 plan to establish close cooperation among participating laboratories and other research
1152 institutions. The software will also need to be amenable to running on Grid facilities,
1153 and will require Distributed Data capability (see 6.5).

1154 **6.5 Distributed Computing, Workload and Workflow Management**
1155

1156 **6.5.1 Scale of the Processed Data**

1157 According to our estimates, the volume of raw data will be in the petabyte range. The
1158 offline data can be classified as follows:

- 1159 • Monte Carlo data, which will contain multiple event samples to cover various event
1160 types and other conditions during the measurements with the prototype detector
- 1161 • Data derived from Monte Carlo events, and produced with a variety of tracking
1162 and pattern recognition algorithms in order to create a basis for the detector
1163 characterization
- 1164 • Intermediate calibration files, derived from calibration data
- 1165 • Processed experimental data, which will likely exist in a few branches correspond-
1166 ing to a few reconstruction algorithms being applied, with the purpose of their
1167 evaluation

1168 In the latter, there will likely be more than one processing step, thus multiplying
1169 data volume. There is sometimes a question about how much of the raw data should be
1170 preserved in the processed data streams. Given a relatively large volume of raw data, the
1171 answer in this case will likely be “none” - for practical reasons, meaning that the derived
1172 data will be just that, and that the size of the processed data will likely by significantly
1173 smaller than the input (the raw data). Given consideration presented above, we will
1174 plan for \sim 1PB of tape storage to keep the processed data. For efficient processing, disk
1175 storage will be necessary to stage a considerable portion of both raw data (inputs) and
1176 one or a few steps in processing (outputs).

1177 Extrapolating from our previous experience running Monte Carlo for the former
1178 LBNE Far Detector, we estimate that we’ll need a few hundred TB of continuously
1179 available disk space. In summary, we request 2PB of disk storage at FNAL to ensure
1180 optimal data availability and processing efficiency. Access to distributed data is discussed
1181 below.

1182 **6.5.2 Distributed Data**

1183 We foresee that data analysis (both experimental data and Monte Carlo) will be per-
1184 formed by collaborators residing in many institutions and geographically dispersed. In
1185 our estimated above, we mostly outlined storage space requirements for major data
1186 centers like CERN and FNAL. When it comes to making these data available to the
1187 researchers, we will utilize a combination of the following:

- 1188 • Managed replication of data in bulk, performed with tools like Spade discussed
1189 above. Copies will be made according to wishes and capabilities of participating
1190 institutions.

- 1191 ● Network-centric federated storage, based on XRootD. This allows for agile, just-
1192 in-time delivery of data to worker nodes and workstations over the network. This
1193 technology has been evolving rapidly in the past few years, and solutions have been
1194 found to mitigate performance penalty due to remote data access, by implementing
1195 caching and other techniques.

1196 In order to act on the latter item, we plan to implement a global XRootD redirector,
1197 which will make it possible to transparently access data from anywhere. A concrete
1198 technical feature of storage at FNAL is that there is a dCache network running at this
1199 facility, with substantial capacity which can be leveraged for the needs of the CERN
1200 prototype analysis. This dCache instance is equipped with a XRootD “door” which
1201 makes it accessible to outside world, subject to proper configuration, authentication and
1202 authorization.

1203 As already mentioned, we plan to host copies of a significant portion of raw and derived
1204 data at Brookhaven National Laboratory, where substantial expertise exists in the field of data handling and processing at scale, due to the principal role this
1205 Laboratory plays in both RHIC (e.g. STAR) and ATLAS experiments. Initial simple
1206 tests of XRootD federation to access data residing at FNAL, from a XRootD instance
1207 located at BNL have been successful. At this point in time we are formulating the
1208 hardware requirements that need to be fulfilled in order for BNL to play the role of an
1209 additional data center as described here.

1211 **6.5.3 Distributed Processing**

1212 At the time of writing, FNAL provides the bulk of computational power for LBNE (not
1213 to mention a few other IF experiments), via Fermigrid and other facilities. We plan to
1214 leverage these resources to process the prototype data. At the same time, we envisage a
1215 more distributed computing model where Grid resources are available transparently and
1216 sometimes on the opportunistic basis, using facilities made available by national Grids
1217 and in the case of the United States, by the Open Science Grid Consortium.

1218 There are currently very large uncertainties regarding what scale of CPU power will
1219 be required to process the data, given that tracking, reconstruction and other algorithms
1220 are in a fairly early stage of development. The best estimates we have at this point range
1221 from 10 to 100 seconds required by a typical CPU to reconstruct a single event. This
1222 means that utilizing a few thousand cores through Grid facilities, it will be possible to
1223 ensure timely processing of these data.

1224 We have not chosen yet the type of Workload Management System to be used for
1225 the purposes of the CERN prototype test. Currently, many researchers at FNAL are
1226 using the *jobsub* tool, which opens access to Fermigrid and additionally to the Open
1227 Science Grid and Cloud resources. There are other capable (and arguably more sophisticated)
1228 systems being used, for example by the LHC experiments. We plan to conduct
1229 an evaluation of these systems with a view to adopt a different solution if necessary.

1230 **7 CERN neutrino platform test environment [5 pages;**
1231 **David/Jack/Cheng-Ju/Thomas]**

1232 Description of Requirements, layout and constraints

- 1233 • short description of location and orientation of cryostat + cryogenics system in
1234 EHN1 (David)
- 1235 • description of beam line layout (Cheng-Ju)
- 1236 • space for staging, control room, electronics racks, clean room, scaffolding, etc.
1237 (Jack)
- 1238 • power requirements and cooling (Jack ?)
- 1239 • ...

1240 **8 Organization, schedule and cost estimate [~5 pages;**
1241 **Thomas/Greg]**

1242 insert organization, schedule and cost estimates here

- 1243 • schedule
- 1244 • working group structure and distributions of tasks/responsibilities
- 1245 •
- 1246 • list detector components covered by LBNX project
- 1247 • describe sharing of cryostat responsibilities (engineering, contracting); what is ex-
1248 pected
- 1249 • beam line expected to be set up by CERN
- 1250 • beam line monitoring
- 1251 • plans for data analysis and publications
- 1252 • describe overlap/commonalities with WA105 data analysis

1253 **9 Summary [~2 pages; Thomas/Greg]**

1254 this is the summary section

1255 **References**

- 1256 [1] IceCube Data Movement <https://icecube.wisc.edu/science/data/datamovement>.
- 1257 [2] Data processing and storage in the Daya Bay Reactor Antineutrino Experiment
1258 <http://arxiv.org/pdf/1501.06969.pdf>.
- 1259 → total estimated page count: ~60 pages

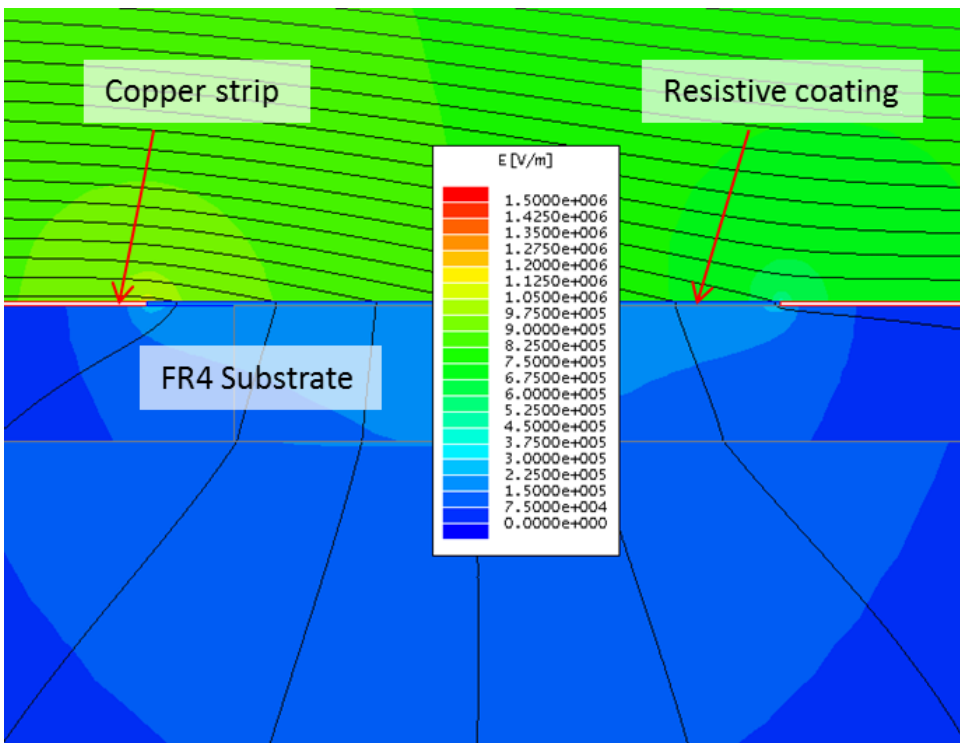


Figure 12: Plot of electric field (color contours) and equi-potential contours (black lines) in a small region around the edges of two adjacent field cage strips on a 1.6mm thick FR4 substrate. A layer of resistive coating between the two copper strips nearly eliminated the high electric field regions at the copper edges.

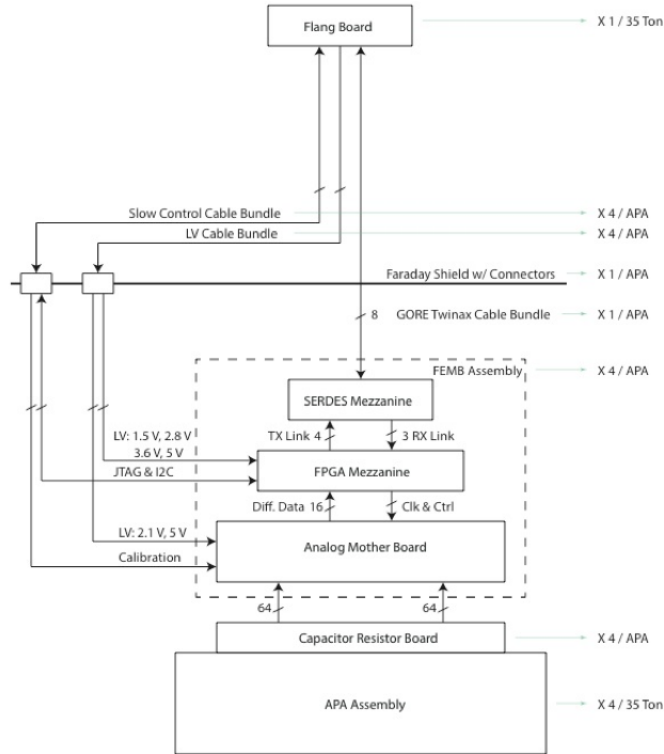


Figure 13: Schematic for the TPC cold FE electronics. ***MG*** Not sure if this is high enough quality. ***Ask Chen for source and fix numbers.

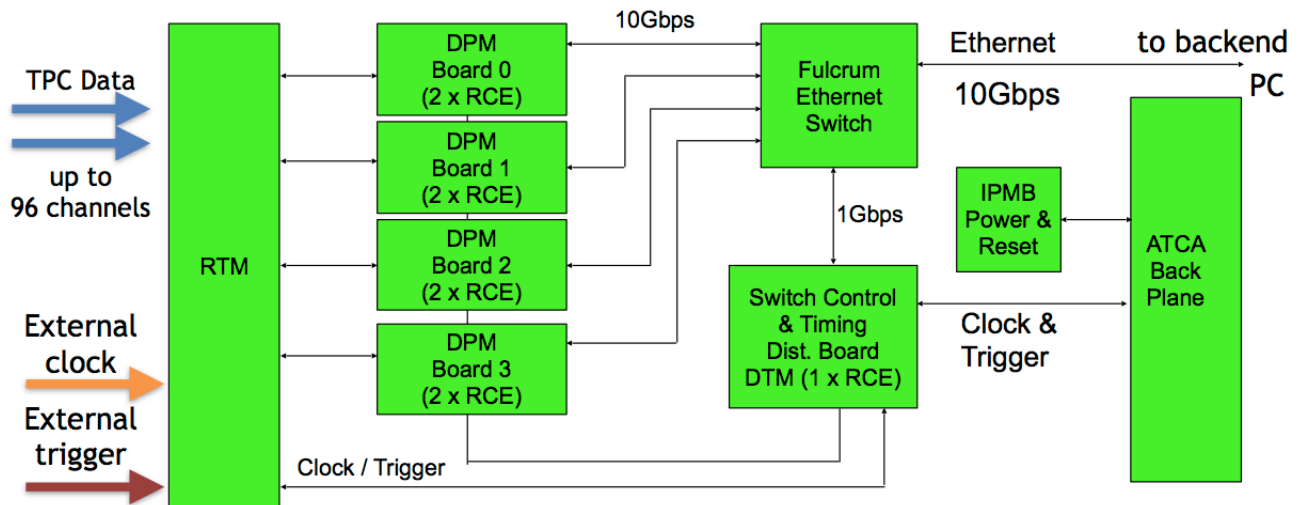


Figure 14: Schematic for the TPC DAQ system.

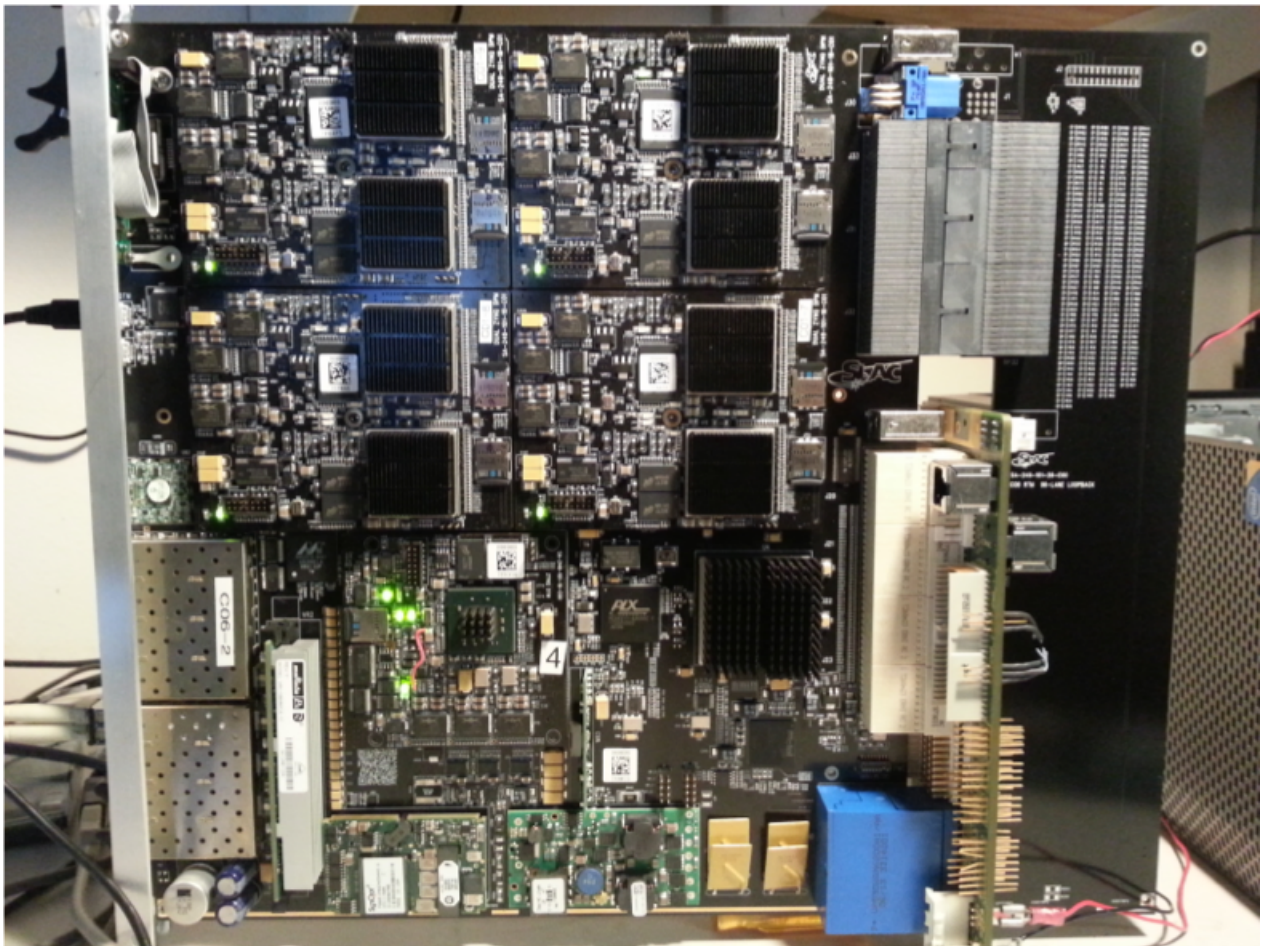


Figure 15: The COB (left of the large connectors) and RTM (right).

GST® Containment System

AS A PRIMARY BARRIER :

a flexible (1.2mm) stainless steel membrane



The double network of corrugations absorbs the thermal contractions due to the very low temperature of the LNG.

Insulating panel

The thickness of the panels can be adjusted to provide a large range of boil-off rates according to the operator's requirements (typically 0.05% per day).

Plywood

Reinforced polyurethane foam

AS A SECONDARY BARRIER :

a composite laminated material

This consists of a thin sheet of aluminium between two layers of glass cloth and resin.

In the event of a failure of the primary membrane, it prevents the build-up of stress concentrations on concrete corner and ensures the liquid tightness of the concrete wall.

Reinforced polyurethane foam

Plywood

Mastic

Post-tensionned concrete covered by a moisture barrier

The outer concrete container provides the *structural resistance* to internal (LNG hydrostatic & dynamic pressure, and vapour gas pressure) and external (wind, snow, ice) loads.

A moisture barrier, applied on its inner side, prevents moisture from entering the tank.

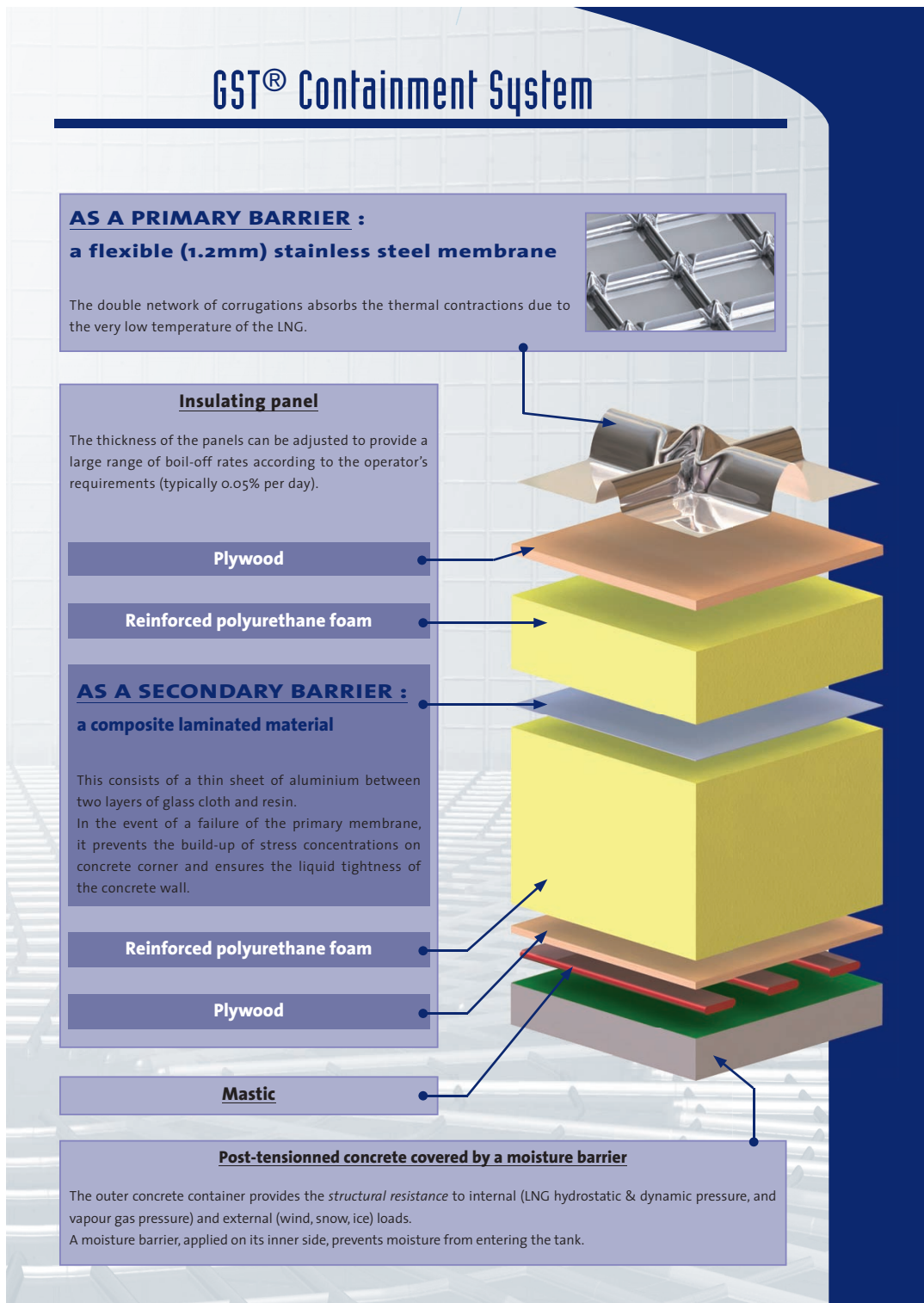


Figure 16: Exploded view of the membrane cryostat technology

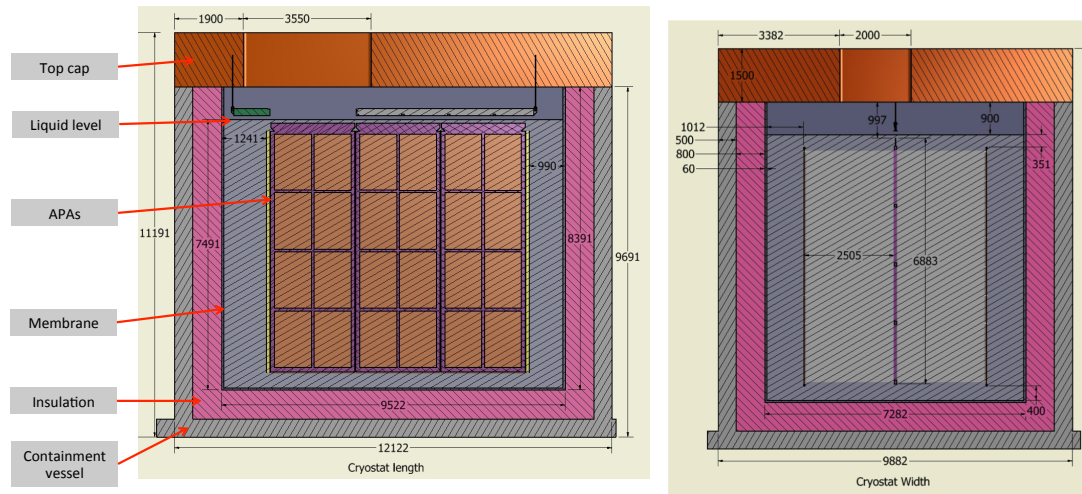


Figure 17: Side (left) and end (right) views of cryostat

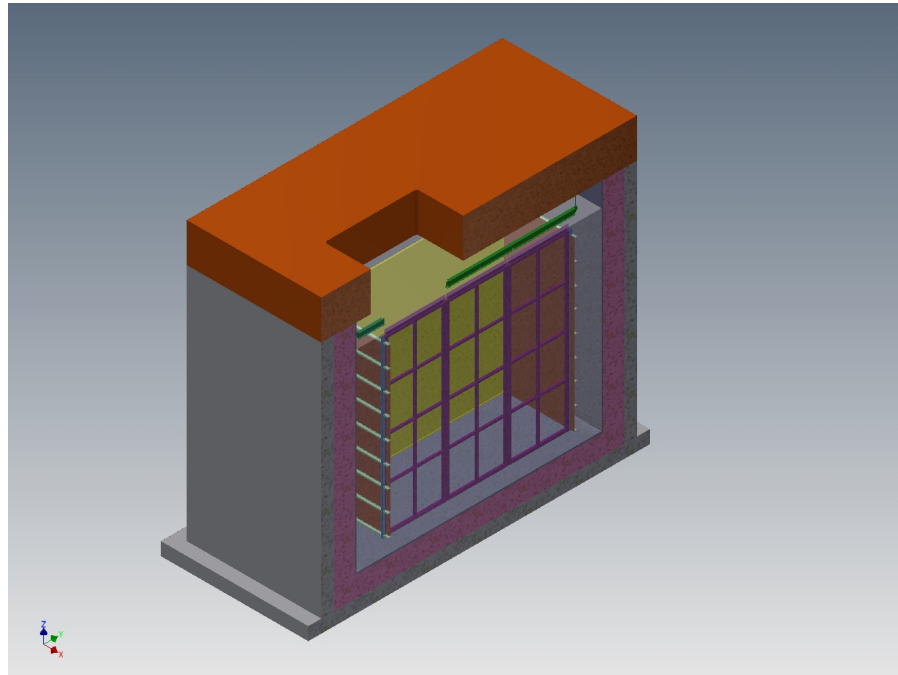


Figure 18: Isometric view of the membrane cryostat

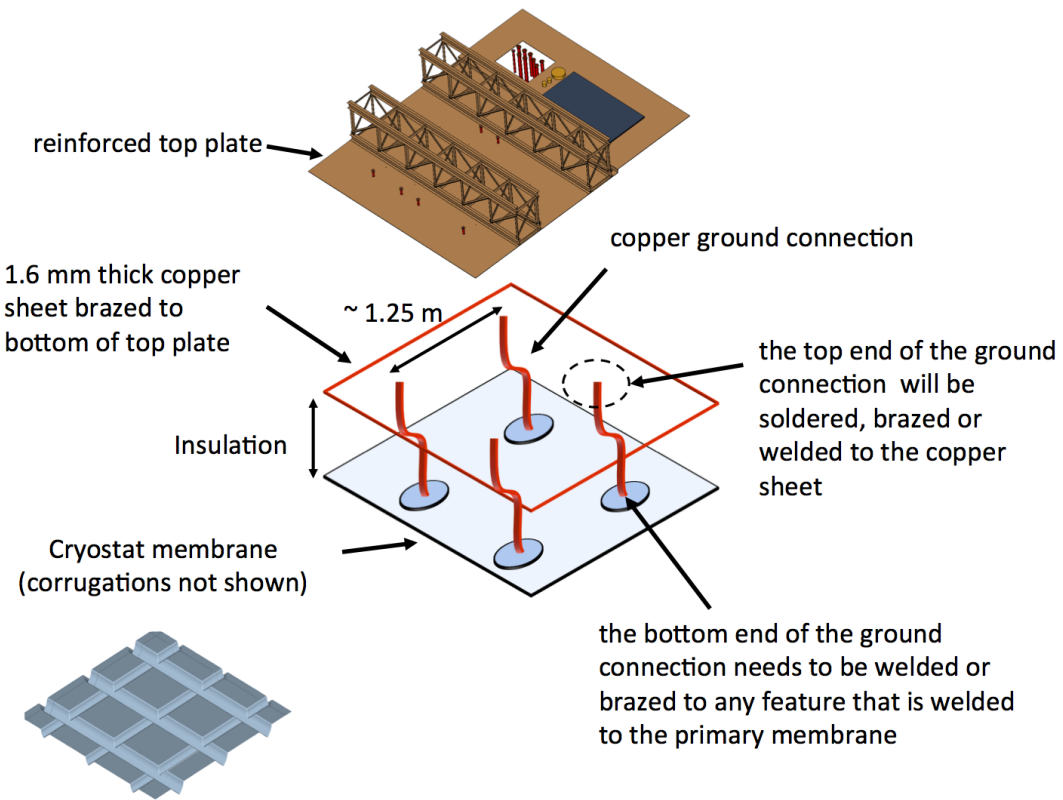


Figure 19: Top plate grounding layout

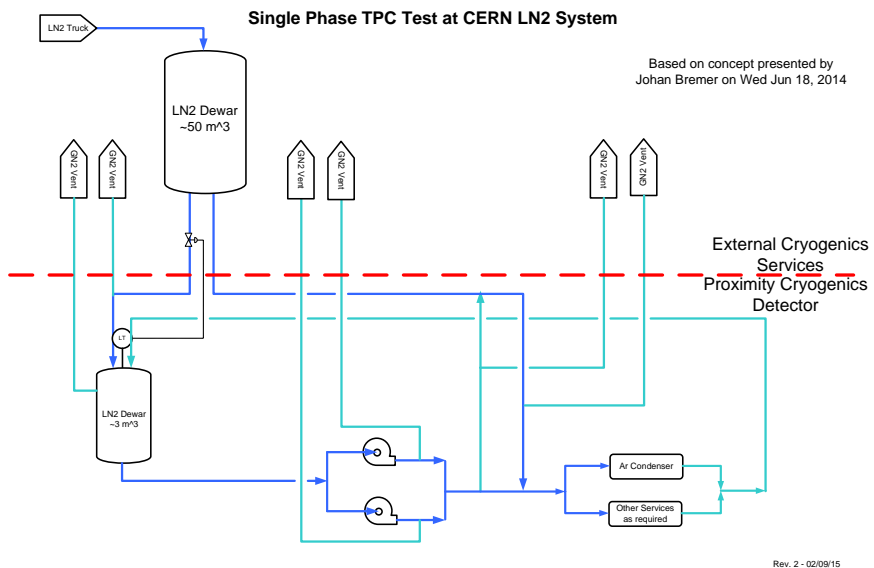


Figure 20: Schematic diagram for the proposed LN2 system

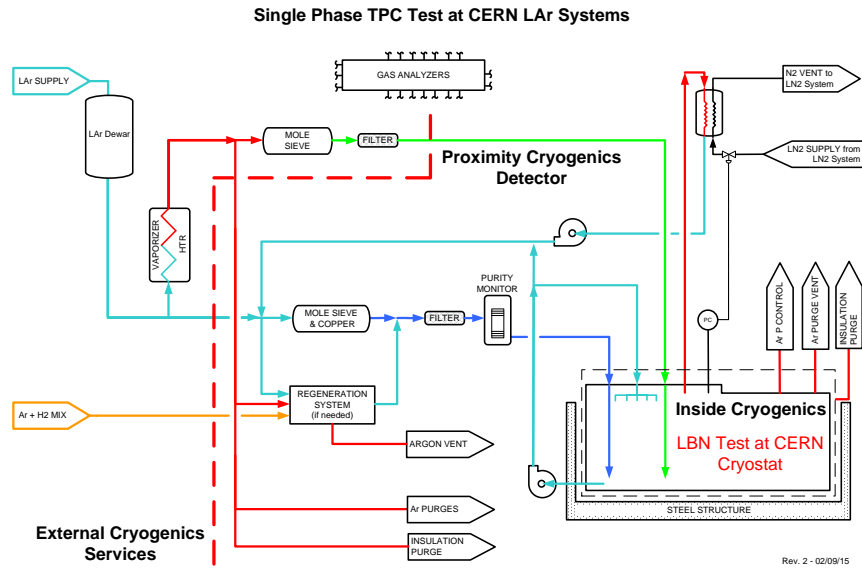


Figure 21: Schematic diagram for the proposed LAr system

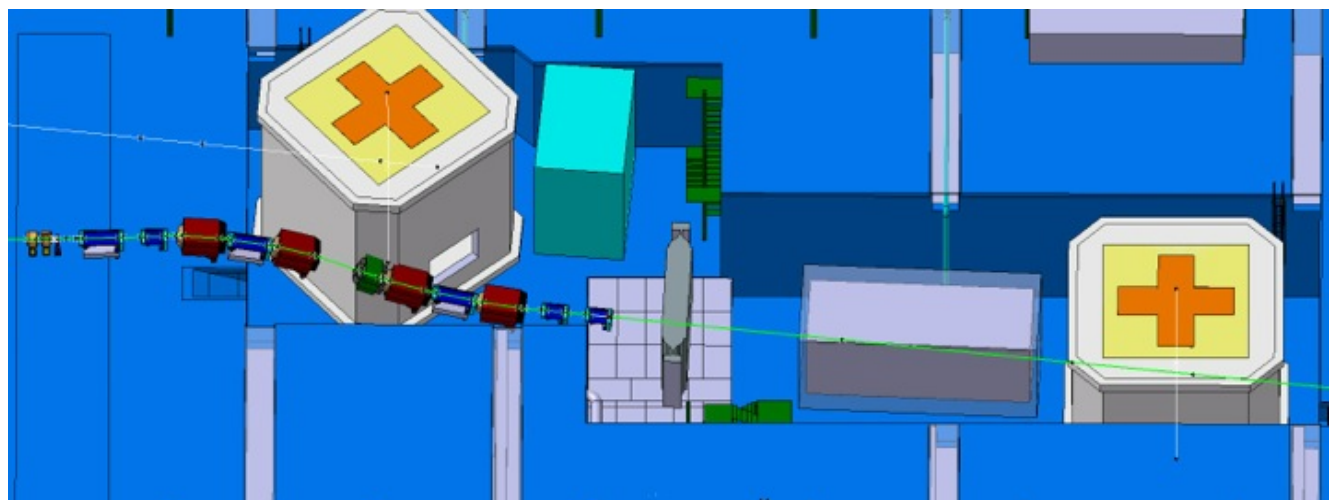


Figure 22: Preliminary layout of the H4ext beamline